NBO, HOMO, LUMO analysis and Vibrational spectra (FTIR and FT Raman) of 1-Amino 4-methylpiperazine using *ab initio* HF and DFT methods

G. Mahalakshmi, V. Balachandran

PII: S1386-1425(14)01056-7
DOI: http://dx.doi.org/10.1016/j.saa.2014.06.157
Reference: SAA 12416

To appear in: *Spectrochimica Acta Part A: Molecular and Biomolecular Spectroscopy*

Received Date: 27 April 2014
Revised Date: 17 June 2014
Accepted Date: 30 June 2014

Please cite this article as: G. Mahalakshmi, V. Balachandran, NBO, HOMO, LUMO analysis and Vibrational spectra (FTIR and FT Raman) of 1-Amino 4-methylpiperazine using *ab initio* HF and DFT methods, *Spectrochimica Acta Part A: Molecular and Biomolecular Spectroscopy* (2014), doi: http://dx.doi.org/10.1016/j.saa.2014.06.157

NBO, HOMO, LUMO analysis and Vibrational spectra (FTIR and FT Raman) of 1-Amino 4-methylpiperazine using *ab initio* HF and DFT methods

G. Mahalakshmi[a,b], V. Balachandran[c*]

[a]Department of Physics, Karpagam University, Coimbatore 641021, India

[b]Department of Physics, Government Arts College(Autonomous), Karur 639 005, India

[c] Research Department of Physics, Arignar Anna Government Arts College, Musiri, Tiruchirapalli 621211, India

Abstract

Experimental FTIR and FT-Raman spectroscopic analysis of 1-Amino-4-methylpiperazine (1A4MP) have been performed. A detailed quantum chemical calculations have been carried out using ab initio HF and density functional theory calculations (B3LYP) with 6–311+G(d,p) basis set. The atomic charges, electronic exchange interaction and charge delocalization of the molecule have been performed by natural bond orbital (NBO) analysis. Electron density distribution and frontier molecular orbitals (FMOs) have been constructed at B3LYP/6–311+G(d,p) level to understand the electronic properties. The charge density distribution and site of chemical reactivity of the molecule have been obtained by mapping electron density isosurface with electrostatic potential surfaces (ESP). The electronic properties, HOMO and LUMO energies were measured by time-dependent TD-DFT approach. The dipolemoment (μ), polarizability (α), anisotropy polarizability ($\Delta\alpha$) and hyperpolarizability (β) of the molecule have been reported.

Keywords:

FT-IR

FT-Raman

HF/DFT studies

NBO

HOMO-LUMO

1-Amino-4-methylpiperazine

* Corresponding author. Tel.: +91 431 2432454; fax: +91 4326 262630.

E–mail address: brsbala@rediffmail.com. (V. Balachandran)

1. Introduction

Piperazine is a heterocyclic compound containing four carbon atoms and two of nitrogen at 1st and 4th position (also called 1, 4-Hexahydropyrazine). It is a deliquescent crystalline compound. It is used as a main ingredient of anthelmintics, which is used to treat intestinal roundworms (ascariasis) infection in human and poultry and to treat pinworms (enterobiasis, oxyuriasis) by altering cell membrane permeability and causing hyperpolarization of the membrane. Piperazine is a moiety in psychoactive drugs. Certain piperazine derivatives are suspected of ecstasy substitutes. Benzylpiperazine is banned in many countries. Benzylpiperazine has been used as an anthelmintic (antiparastic effect). Nitrogen in piperazine ring plays an important role in biological research and drug manufacturing industry including the preparation of anthelmintic, antiallergenic, antibacterial, antihistamic, antiemetic and antimigraine agents. The piperazine ring and piperazine derivatives are important cyclic components in industrial field as raw materials for hardener of epoxy resins, corrosion inhibitors, insecticides, accelerators for rubber, urethane catalysts, and antioxidants. An example of 1-Amino-4-methylpiperazine application is to be used as an intermediate for pharmaceuticals (Anti-tuberculostatic agent: Rifampicin). Studies of amino group by vibrational spectroscopy are very useful in obtaining information regarding the molecular confirmation and the nature of hydrogen bonding in biologically important substances [1, 2].

Literature survey reveals that to the best of our knowledge, the results based on quantum chemical calculation, FT-IR and FT-Raman spectral studies, HOMO-LUMO and NBO analysis on 1-Amino-4-methylpiperazine (1A4MP) have no reports. Due to this scantiness observed in the literature persuaded us to make this theoretical and experimental vibrational spectroscopic research to give a correct assignment of the fundamental bands in the experimental FTIR and FT-Raman spectra, on the basis of the calculated potential energy distribution (PED) using Pulay's DFT based on scaled quantum chemical approach. Moreover, the effects have been taken to predict a complete description of the molecular geometry, vibrational frequencies, structural confirmation stability, atomic charges, natural bond orbital (NBO) analysis and HOMO-LUMO energies of 1A4MP.

2. Experimental process

The title compound was obtained from the Lancaster Chemical Company, UK and used for the spectral measurements without further purification. The room temperature FT-IR spectrum of the title compound was recorded in the region 400–4000 cm^{-1}, using a BRUKER IFS 66V FTIR spectrometer, equipped with an MCT detector, a KBr beam splitter and a globar source. FT-Raman

spectrum of 1A4MP were recorded on the same instrument with FRA 106 Raman accessories in the region 0–4000 cm^{-1}. The 1064 nm line of a Nd:YAG laser for excitation operating at 1.5 W power.

3. Computational methods

Quantum chemical calculations were used to carry out the optimized geometry and vibrational wavenumbers of 1A4MP with 2009 version of the Gaussian suite program [3] using the HF and DFT functional [4, 5] supplemented with 6−311+G(d,p)basis sets. Scaling of the force field was performed according to the SQM procedure [6, 7] using selective scaling in the natural internal coordinate representation [8]. The vibrational frequencies calculated at DFT method with 6−311+G(d,p) level of basis set were scaled by 0.9401 for wavenumbers less than 1000 cm^{-1} and 0.9610 wavenumber greater than 1000 cm^{-1}. The scaled values used in HF/6−311+G(d,p) were 0.8451 for wavenumbers less than 1000 cm^{-1} and 0.9101 for wavenumber greater than 1000 cm^{-1}. After scaling factor, the deviation from the experiment value is more reliable. Transformation of the force field and subsequent normal coordinate analysis including the least square refinement of the scale factors, calculation of the potential energy distribution [PED] and the prediction of FT-IR and FT-Raman intensities were done on a PC with the MOLVIB Program (version 7.0G77) written by Sundius [9,10]. From the basic theory of Raman scattering, Raman activities (s_i) calculated by Gaussian 09 program has been converted to relative Raman intensities (I_i) using the following relationship:

$$I_i = \frac{f(\upsilon_0 - \upsilon_i)^4 s_i}{\upsilon_i[1 - \exp(-hc\,\upsilon_i)]/kT}$$

where

υ_0 is the exciting wave number (in cm^{-1} units)

υ_i is the vibrational wave number of the i^{th} normal mode

h, c, and *k* are universal constants

and *f* is a suitably chosen common normalization factor for all the peak intensities.

A detailed description of vibrational modes can be given by means of normal coordinate analysis. For this purpose, a full set of 69 standard internal coordinates containing 12 redundancies were defined as given in Table 1. From these, a non-redundant set of local symmetry coordinates were constructed by suitable linear combinations of internal coordinates following the recommendations of Pulay et al. [11] and they are presented in Table 2. Natural bond orbital

analysis was also performed by the Gaussian 09 [3] program at the DFT level of theory analysis and it transforms the canonical delocalized molecular orbital's into localized molecular orbital's that are closely tied to chemical bonding concepts. This process involves sequential transformation of non-orthogonal atomic orbital's to the sets of natural atomic orbital's (*NAO's*), natural hybrid orbital's (*NHO's*) and natural bond orbital's (*NBO's*). The localized basis set completely describes the wave functions in the most economic method, as electron density and other properties are described by the minimal amount of filled NBO's, which describe the hypothetical, strictly localized Lewis structure which can be used as the measure of delocalization. This non-covalent bonding and anti-bonding charge transfer interactions can be quantitatively described in terms of the second order perturbation interaction energy ($E^{(2)}$) [12–15]. This energy represents the estimate of the off-diagonal NBO Fock Matrix elements. It can be deduced from the second – order perturbation approach [16] as follows:

$$E^{(2)} = \Delta E_{ij} = q_i \frac{F_{(i,j)}^{2}}{\varepsilon_j - \varepsilon_i}$$

where q_i is the i^{th} donor orbital occupancy, ε_j, ε_i the diagonal elements (orbital energies) and *(j,i)* the off diagonal NBO Fock Matrix element.

4. Results and discussion

4.1 Optimized geometry

The optimized structure of 1A4MP is shown in Fig. 1 with numbering of the atoms. 1A4MP has a structure similar to the chair form of cyclohexane. In order to find out the most optimized geometry, the energy calculations were carried out for various possible conformers. The possible four conformers *cis-cis*(I), *cis-trans*(II), *trans-cis*(III), *trans-trans*(IV) of 1A4MP are shown in Fig.2. It is clear from Fig. 2 that the conformer *trans-cis*(III) has produced the global energy minimum. The most optimized geometrical parameters were calculated for 1A4MP of *trans-cis*(III) conformer by HF and B3LYP methods with 6-311+G(d,p) basis set. The bond lengths and bond angles are determined from geometrical parameters obtained from HF and DFT method. The calculated global minimum energy of 1A4MP in C1 point group symmetries are –9803.9693 and –9868.623651 eV by HF and DFT methods, respectively. The optimized structure can be compared with other similar systems [17] for which the crystal structures have been solved. The optimized bond lengths and bond angles of the title compound which is calculated using HF and DFT methods with 6–311+G(d,p) basis set are shown in Table 3. From the experimental values of literature [17],

C–C single bond length is 1.51 Å and C–N single bond length is 1.45 Å for N-(4-Chlorophenyl)-4-methylpiperazine-1-carboxamide. The molecule of 1A4MP has two substituents such as the methyl and amide group, attached to a non-planar piperazine ring. Amide group and piperazine ring have non-planar structures, therefore C1 point group symmetry is used for computation.

The calculated structural parameters for 1A4MP are listed in Table 3. Among the different conformers of cyclohexanone, the chair form is energetically favored [18]. The computed values of torsion angles C6–N1–C2–C3, C2–N1–C6–C5, N1–C2–C3–N4, C2–C3–N4–C5, C3–N4–C5–C6, and N4–C5–C6–N1 are -51.96^0, 52.26^0, 54.53^0, -56.43^0, 56.90^0, and -55.27^0 respectively. It can be concluded that the chair form arises due to the van-der Waals' repulsion between the hydrogen atoms belonging to neighboring carbon atoms. In order to reduce the steric repulsion the bond angles are expanded to C5–N4–C14, C3–N4–C14, C6–N1–N7 and C2–N1–N7 at 112.06^0, 112.03^0, 110.64^0 and 114.50^0, respectively.

The van-der Walls repulsion of H13, H18 with H16 and, H13, H18 with H9 causes a steric hindrance in achieving co-planarity for piperazine ring with the CH_3 and NH_2 groups. Hence the CH_3 and NH_2 groups assumes the dihedral angles N7–N1–C6–C5 (-75.99^0), N7–N1–C2–C3 (74.38^0) and C14–N4–C5–C6 (-176.19^0), C14– N4–C3–C2 (176.60^0). In the compound, the atoms N7 and C14 are slightly distorted from the plane and the two groups are flipped.

4.2 Static polarizability, first and second order hyperpolarizability

NLO techniques are considered as among the most structure sensitive methods to study the molecular structures [19] and the computational approach allows the determination of molecular NLO properties as an inexpensive way to design molecules by analyzing the potential before synthesis and to determine high-order hyperpolarizability tensors of molecules. In the recent years, because of potential applications in modern communication technology, data storage, telecommunication, and optical signal processing, a large number research of new materials exhibiting efficient nonlinear optical (*NLO*) properties has been of great interest [20, 21]. It is known that the significance of the polarizability and the first hyperpolarizability of molecular systems are dependent on the efficiency of electronic communication between acceptor and the donor groups as that will be the key to intramolecular charge transfer [22, 23]. The acceptor and donor groups have an important role in the polarizability and first hyperpolarizability. The large value of first hyperpolarizability, which is the measure of the NLO activity of the molecular system, is associated with the Intra molecular Charge Transfer (ICT), resulting from the electron cloud

movement through π conjugated frame work from electron donor to electron acceptor groups [24]. The polar properties of the title molecule were calculated at the DFT/6−311+G(d,p) level.

The simplest polarizability (α), characterizes the ability of an electric field to distort the electronic distribution of a molecule. Higher order polarizabilities (hyperpolarizabilities β, γ…) which describe the non−linear response of atoms and molecules are related to a wide range of phenomena from non-linear optics to intermolecular forces, such as the stability of chemical bonds, as well as, the conformation of molecules [25]. They made possible the determination of the elements of these tensors from derivatives of the dipolemoment with respect to the electric field. The first hyperpolarizability (β_0) and related properties (β, α_0 and $\Delta\alpha$) are calculated based on the finite−field approach. In the presence of an applied electric field, the energy of a system is a function of the electric field. The first hyper polarizability is a third−rank tensor that can be described by a 3x3x3 matrix. The 27 components of the 3D matrix can be reduced to 10 components due to the Kleinman symmetry [26]. The components of β are defined as the coefficients in the Taylor series expansion of the energy in the external electric field. When the electric field is weak and homogeneous, this expansion becomes,

$$E = E^0 - \mu_i F_i - 1/2\ \alpha_{ij} F_i F_j - 1/6\ \beta_{ijk} F_i F_j F_k - 1/24\ \gamma_{ijkl} F_i F_j F_k F_l + \ldots$$

where E^0 is the energy of the unperturbed molecules, F_i is the field at the origin and μ_i, α_{ij}, β_{ijk} and γ_{ijkl} are the components of dipolemoment, polarizability, first and second order hyperpolarizability respectively. These studies led to the fact that *ab initio* calculations of polarizabilities and hyper polarizabilities have become available through the strong theoretical basis for analyzing molecular interactions. They made possible the determination of the elements of these tensors from derivatives of the dipolemoment with respect to the electric field.

The density functional theory (DFT) provides a convenient theoretical frame work for calculating global and local indices that quantitatively describe the inherent activity of chemical species. The dipolemoment can be extracted from the output of any standard electronic structure program. Many experiments are done on isotropic systems (gases, neat liquids, and solutions) where the invariant vector and scalar components are measured [27]. The total static dipolemoment μ, the mean polarizability α_0, the anisotropy of the polarizability $\Delta\alpha$ and the mean first hyper polarizability β_0, using the x−, y− and z− components are defined as

$$\mu = \sqrt{\left(\mu_x^2 + \mu_y^2 + \mu_z^2\right)}$$

$$\alpha_o = \frac{\alpha_{xx} + \alpha_{yy} + \alpha_{zz}}{3}$$

$$\Delta\alpha = 2^{-1/2}\left[(\alpha_{xx} - \alpha_{yy})^2 + (\alpha_{yy} - \alpha_{zz})^2 + (\alpha_{zz} - \alpha_{xx})^2 + 6\alpha_{xx}^2\right]^{1/2}$$

The other components of the polarizability (α_{xy}, α_{xz}, *etc*.) are not needed to obtain the isotropic quantity. The dipolemoment μ, the mean polarizability α_0 are calculated using Gaussian 09 software and is found to be 1.706 Debye and 0.593×10^{-24} e.s.u., respectively. The first order hyper polarizability β was also calculated using the finite field approach theory. The components of first hyperpolarizability can be calculated using the following equation

$$\beta_i = \beta_{ijk} + \frac{1}{3}\sum(\beta_{ijj} + \beta_{jij} + \beta_{jji}), (i \neq j)$$

Using the x, y and z components, the magnitude of the first hyperpolarizability tensor can be calculated using

$$\beta_{total} = \sqrt{(\beta_x^{\,2} + \beta_y^{\,2} + \beta_z^{\,2})}$$

The complete equation for calculating the magnitude of the first hyperpolarizability from Gaussian 09 output is as follows.

$$\beta_x = \beta_{xxx} + \beta_{xyy} + \beta_{xzz}$$
$$\beta_y = \beta_{yyy} + \beta_{xxy} + \beta_{yzz}$$
$$\beta_z = \beta_{zzz} + \beta_{xxz} + \beta_{yyz}$$

The first and second order hyperpolarizability of 1A4MP calculated and is found to be 1.144797×10^{-35} *e.s.u.* and -39.514×10^{-35} *e.s.u*. The equation for average second hyperpolarizability is

$$\langle\gamma\rangle = \frac{1}{5}(\gamma_{xxxx} + \gamma_{yyyy} + \gamma_{zzzz} + 2\gamma_{xxyy} + 2\gamma_{xxzz} + 2\gamma_{yyzz})$$

The theoretical first and second order hyperpolarizability was calculated using Gaussian 09 software. Since the value of the polarizability and hyperpolarizability of Gaussian 09 output are reported in a atomic mass units (a.u.), the calculated values have been converted into electrostatic units (esu) (α: 1 a.u. = 0.1482×10^{-24} esu; β: 1 a.u. = 8.6393×10^{-33} esu). The calculated values of α, β and γ and the corresponding components are given in Table 4. Urea is one of the prototypical molecules used in the study of the NLO properties of molecular systems. Therefore it was used

frequently as a threshold value for comparative purposes. The calculated first hyperpolarizability of 1A4MP is 1.14.47 x10^{-35} esu which is 3.2 times smaller than urea (0.37189 x10^{-30} esu).

4.3 NBO analysis

NBO results showing the formation of Lewis and non–Lewis orbital by the valence hybrids corresponding to the intramolecular bonds are given in Table 5. In addition the most important interactions between 'filled' (donors) Lewis–type NBOs and 'empty' (acceptors) non–Lewis NBOs are also reported.

In NBO analysis large $E^{(2)}$ value shows the intensive interaction between electron–donors and electron–acceptors and greater the extent of conjugation of the whole system. The most important possible intensive interactions are given in Table 5. The second order perturbation theory analysis of Fock matrix in NBO basis shows strong intramolecular hyperconjugative interactions of π electrons. There is strong intramolecular hyperconjugative interaction of π electrons in the aromatic ring, i.e. C3–N4 and N4–C5 bonds conjugate to the π*(N4–C14) bond of piperazine ring. The electron density (*ED*) 0.03347 e leads to a stabilization energy 12.44 kJ mol^{-1}. This enhancement of π*(N4–C14) NBO further conjugates with π*(C3–N4) and π*(N4–C5) resulting to a stabilization energy of 10.19 and 10.21 kJ mol^{-1}, respectively.

The hyperconjugative interaction between the nitrogen lone pair and C–H antibonding orbital of the methyl is maximum, i.e. L(1)N4→π*(C14–H16) increases ED in C–H antibonding orbital (0.12058 e) that weakens the respective bond (C14–H16= 1.0961 Å) leading to stabilization energy of 50.58 kJ mol^{-1}. The most important interaction energy related to the resonance of the molecule is electron donation from n(1)N4 (1.7298 e) to the antibonding acceptor orbitals π*(1) C2–C3 (4.25 kJ mol^{-1}) and π*(1) C5–C6 (4 kJ mol^{-1}). These interactions lead to stability and in turn to the bioactivity of 1A4MP.

Furthermore, the NBO analysis of 1A4MP gives the evidence for the formation of strong and very week intramolecular interactions between nitrogen loan electron pairs and π*(C–H), π*(C–C) antibonding orbitals. In Table 6, the occupation numbers with their energies for the interacting NBOs are presented. The NBO analysis also describes the bonding in terms of natural hybrid orbital L(1)N4, which occupy a higher energy orbital (–0.2168a.u.) with considerable *p*–character (99.89%) and low occupation number (1.72982a.u.) and the other BD(1)N1–N7 occupy a lower energy orbital (–0.8170a.u.) with p–character (79.9%) and high occupation number (1.9927a.u.). Thus, a very close to pure p–type lone pair orbital participates in the electron donation to the

π*(C–C) and π*(C–C) orbital for nitrogen lone pair to antibonding carbon–carbon and carbon–nitrogen interaction in the compound.

4.4 Atomic charge

The charge distributions calculated by the Mulliken [28] and NBO methods for equilibrium geometry of 1A4MP are given in Table 7. The corresponding Mulliken's plot is shown in Fig. 3. The total charge of the investigated complex is equal to zero. The calculated results reveal that the negative charge is delocalized between carbon and nitrogen atoms. In 1A4MP molecule, the atoms constituting the hydrogen bonds possess the positive charges [29]. While all the carbon atoms in the molecule have negative charges which form the hydrogen bonds, very similar values of positive charges are noticed for the four hydrogen pairs forming the CH_2 groups and one NH_2 group connected with carbon and nitrogen atoms of the piperazine ring. For the hydrogen atoms, the differences in calculated charge are relatively smaller. Very similar values of positive charges are observed for hydrogen atoms connected with carbon atoms of piperazine ring. It is worth mentioning that the biggest values of charge are noticed for H13 and H14 which are involved in hydrogen bonding (0.2279e and 0.2352e, respectively). The charge increase at the hydrogen atoms taking part in hydrogen bonding (as supported by NBO analysis) is also a clear manifestation of hydrogen bonding. Large values of charge on N7 (negative) and H9 (positive) are due to intramolecular charge transfer. Fig. 3 shows that the natural atomic charges are more sensitive to the changes in the molecular structure than Mullikan's net charges.

4.5 HOMO–LUMO energy gap

Spatial distribution of molecular orbitals, especially those of highest occupied molecular orbital (HOMO) and lowest unoccupied molecular orbital (LUMO), are excellent indicators of electron transport in molecular systems. The conjugated molecules are characterized by a small HOMO–LUMO separation, which is the result of a significant degree of ICT from the end–capping electron–donor groups to the efficient electron–acceptor groups through conjugated path. In 1A4MP, the HOMO–LUMO energy gap is -4.09858eV. The lowering of the HOMO–LUMO band gap is essentially a consequence of the large stabilization of the LUMO due to the strong electron–accepting ability of the electron–acceptor group.

The HOMO and LUMO orbitals are shown in Fig. 4. Since the atomic π–orbitals point towards each other and have better overlap, an increase in *p*–character points the fact that sigma bonds are stronger as evidenced by NBO analysis. The positive phase is red and the negative one is green. It is clear from the Fig. 4 that, while the HOMO localizes on the three bond regions (C3–N4, C5–N4 and C14–N4), a highly delocalized HOMO and LUMO indicates that the electrons can more readily move around the molecule and hence an improved ICT. On the other hand, the LUMO strongly localizes on the five different bond regions (N7–H8, N7–H9, N1–N7, N1–C6 and N1–C2) indicating the presence of favorable atomic centers within 1A4MP for possible nucleophilic attacks and its bioactivity. The HOMO→LUMO transition implies an electron density transfer to CH_3 group from the NH_2 group.

The chemical hardness and softness of molecule is a good indicator of the chemical stability of a molecule. From the HOMO–LUMO energy gap, one can find whether the molecule is hard or soft. The molecules having large energy gap are known as hard and molecules having a small energy gap are known as soft molecules. The soft molecules are more polarizable than the hard ones because they need small energy for excitation. The hardness value of a molecule can be determined by the formula

$$\eta = \frac{(-\varepsilon_{HOMO} + \varepsilon_{LUMO})}{2}$$

where ε_{HOMO} and ε_{LUMO} are the energies of the HOMO and LUMO orbitals. The value of η in the title molecule is 2.049eV.

4.6 Molecular electrostatic potential

In the present study, 3D plots of molecular electrostatic potential (MEP) of 1A4MP is illustrated in Fig. 5. The MEP is a plot of electrostatic potential mapped onto the constant electron density surface. The MEP surface is superimposed on top of the total energy density. The MEP is a useful property to study reactivity given that an approaching electrophile will be attracted to negative regions (where the electron distribution effect is dominant). In the majority of the MEPs, while the maximum negative region which is preferred site for electrophilic attack is indicated in red colour, the maximum positive region which is referred site for MEP lies in the fact that it simultaneously displays molecular size, shape as well as positive, negative and neutral electrostatic potential regions, in terms of colour grading (Fig. 5) and is very useful in research of molecular structure

with its physiochemical property relationship [29, 30]. The resulting surface simultaneously displays molecular size and shape and electrostatic potential value.

The different values of the electrostatic potential at the surface are represented by different colours. Potential increases in the order red < orange < yellow < green < blue. The colour code of these maps is in the range between 0.381165a.u. (deepest blue) and –0.974908a.u. (deepest red) in compound, where blue indicates the strongest attraction and red indicates the strongest repulsion. Regions of negative *V(r)* are usually associated with the lone pair of electronegative atoms.

Fig. 5 shows the plot of molecular electrostatic potential surface of 1A4MP along with the computationally derived electrostatic potential and electrostatic point charges on its individual atoms. It is clear from the figure that the atoms N7, C2, H16and H15 holds significant electronegative charges and the atoms H9, H8, 1N and N4 holds significant positive charges. The MEP surface, the negative electrostatic potentials are shown in red color and the intensity of which is proportional to the absolute value of the potential energy, and positive electrostatic potentials are shown in blue. In view of this, we can say that the delocalization of charge and electron density of atoms primarily takes place within the benzene ring and the electron donating amino and methyl substituents increase the chemical reactivity of a molecule.

4.7. Vibrational spectral analysis

The vibrational assignments in the present work are based on the HF and DFT/6-311+G(d,p) frequencies, IR intensities, Raman activities, Raman intensities as well as characteristic group frequencies. In agreement with C_1 symmetry, all the 57 vibrations are distributed as 21 stretching vibrations, 18 in-plane and 18 out-of-plane vibrations of same symmetry species. The observed (FT-IR and FT-Raman) spectra are shown in Fig. 6. The detailed vibrational assignments of fundamental modes of 1A4MP along with observed and calculated frequencies and normal mode descriptions have been reported in Table 8. It is convenient to discuss the vibrational spectra of 1A4MP in terms of characteristic spectral region as describe below.

4.7.1 Vibrations of amine group

The methyl and amino groups are generally referred as electron donating substituents in aromatic ring systems [31]. The NH_2 group gives rise to the six internal modes of vibrations such as: the symmetric stretching, the antisymmetric stretching, the symmetric deformation or the scissoring, the rocking, the wagging and the torsional modes. The molecule under investigation possesses only one NH_2 group and hence expects one symmetric and one asymmetric N–H

stretching vibrations in NH_2 group. The antisymmetric stretching for the CH_2, NH_2 and CH_3 has magnitude higher than the symmetric stretching [32]. The symmetric stretching, the antisymmetric stretching modes are easily assigned owing to their characteristic magnitudes in amino substituted benzenes. For saturated amines, it is established that the asymmetric NH_2 stretch will give rise to a band between 3300–3500 cm^{-1} [33]. The infrared spectrum shows a weak band observed at 3390 cm^{-1} corresponding to NH_2 asymmetric stretching mode. The symmetric stretching also observed as weak intense shoulder in Raman spectrum at 3270 cm^{-1}. The *ab initio* computations give the frequency of these bands at 3389 cm^{-1} for NH_2 asymmetric stretch and 3268 cm^{-1} for the symmetric stretch. The observed NH_2 stretching frequencies are higher from the computed frequencies due to the steric interactions (dependents upon the substituents 'position -- axial or equatorial).

For NH_2 scissoring deformation appears in the region 1638–1575 cm^{-1} [34]. The observed band in IR spectrum at 1586 cm^{-1} and corresponding Raman bands at 1583 are attributed to the scissoring mode of the NH_2 group. The calculated frequency for the scissoring mode of NH_2 is 1575 cm^{-1} for 1A4MP, which is coupled with ring stretching mode and it arises mainly due to the HNH and NNH angle bending motions with small contributions from ring stretching and N–NH_2 stretching modes. The computed NH_2 scissoring vibration is in excellent agreement with the recorded spectral data. The observed band at 1424 cm^{-1} in HF and 1399 cm^{-1} in DFT spectrum correspond to the N–NH_2 stretching. The rocking mode of the NH_2 group appears in the range 1000–1100 cm^{-1} with variable IR intensity [35]. The observed weak band at 1074 cm^{-1} in IR spectrum and 1076 cm^{-1} in Raman spectrum are attributed to the appreciable contribution from the NNH angle bending suggesting its origin due to the rocking mode. The wagging mode of the NH_2 group appears in the range 600–800 cm^{-1}. The observed strong band at 788 cm^{-1} in IR spectrum and the band at 792 cm^{-1} in Raman spectrum correspond to the NH_2 wagging mode. The observed weak bands at 298 cm^{-1} in Raman spectrum is assigned to the torsional mode of amino group vibration.

4.7.2 N–N vibrations

In the vibrational analysis of 4, 5-dichloro-3-hydroxypyridazine, Krishnakumar et al. [36] identified the N–N stretching mode at 1374 cm^{-1} in FT-IR and 1380 cm^{-1} in FT-Raman spectra. Hence, in the present study, the FT-Raman band at 1383cm^{-1} is assigned to N–N stretching mode of vibration.

4.7.3 C–N vibrations

The assignment of C–N stretching frequency is a rather difficult task since there are problems in identifying these frequencies from other vibrations. Silverstein *et al*. [37] assigned C–N stretching vibrations in the region 1382–1266 cm^{-1} for the aromatic amines. For N-Methylmaleimide, Parker [38] observed the bands at 1388 and 1254 cm^{-1} in FT-IR and at 1384 and 1254 cm^{-1} in FT-Raman and assigned to C–N symmetric and asymmetric stretching vibrations, respectively. The bands obtained at 1275, 1243 cm^{-1} in FT-IR spectrum and 1271, 1241cm^{-1} in FT-Raman spectra have been assigned to C–N stretching vibrations. The PED contribution results at the last column of Table 8 shows C–N stretching vibrations (48%) interacting considerably with N–N (27%) stretching mode. In the present work, the observed value at 730 and 714 cm^{-1}in FT-IR and FT-Raman spectra was assigned to N–CH_3 stretching vibration. In the present study, the theoretically computed values belonging to C–N stretching vibrations are in agreement with spectral data. The FT-IR and FT-Raman in-plane bending mode (at 949 and 958 cm^{-1}, respectively) corresponding to N–CH_3 moiety was calculated at 969 cm^{-1} with DFT method agree with experiment value.

4.7.4 Methyl group vibrations

The position of the CH_3 vibration is almost entirely dependent upon the nature of the element to which the methyl groups are attached. The title compound possesses a single CH_3 group in fourth position of the piperazine ring. For the assignments of CH_3 group frequencies one can expect nine fundamentals viz., namely the symmetrical stretching in CH_3 (CH_3 sym. stretch), asymmetrical stretching (CH_3asym. stretch), symmetrical (CH_3 sym. deform) and asymmetrical (CH_3asy. deform) deformation modes, in-plane rocking (CH_3ipr), out-of-plane rocking (CH_3opr), CH_3 wagging (CH_3 wag.) and twisting ($CH_{3\ twist}$) modes. Methyl groups are generally referred as an electron donating substitution in the aromatic ring system.

The asymmetric C–H methyl group stretching vibrations are generally observed in the range 2980
cm^{-1} and the symmetric stretching is expected at 2870 cm^{-1} [39,40]. The methyl asymmetric stretching is observed as a strong band in IR at 2954 cm^{-1} and at 2952 cm^{-1} in Raman and the symmetric stretching mode is observed as a strong sharp band at 2920 cm^{-1} in IR and at 2901 cm^{-1} in Raman. The blue shifting (50 cm^{-1}) of methyl symmetric stretching is due to the electron donating inductive effect and hyper conjugative effect {σ(C14–H17) →σ*(C3–N4) and σ(C14–H17)→σ*(N4–C5) bond} of methyl group attached to the aromatic ring [41, 42]. These

effects imply electron delocalization, which may be taken into account by a molecular orbital approach. This can point to changing polarizability and dipolemoment due to electron delocalization [43]. The methyl deformation modes mainly coupled with the in-plane bending vibrations and are also well established. The in-plane methyl deformation mode of 1A4MP is found at 1459 cm^{-1} in FT-IR spectrum and 1438 cm^{-1} in Raman spectrum. The band at 1320 cm^{-1} in FT-IR and 1321cm^{-1} in FT-Raman spectra is attributed to CH_3 out-of-plane deformation mode of 1A4MP. The CH_3 rocking mode is observed at 1045 and 1059 cm^{-1} for 2Cl6MA by Shanker et al.[44]. This band obtained at 1055 cm^{-1} with DFT method is in agreement with experimental value. These vibrational frequencies were observed to be 1046 cm^{-1} in FT-IR and 1042cm^{-1} in FT-Raman spectra are assigned to CH_3 in-plane mode. The out-of-plane rocking mode is observed at 1022 and 1038 cm^{-1} in FT-IR and FT-Raman spectra, respectively. The contributions for all these modes are about 85%. In the present study, they show good agreement with the calculated values.

4.7.5Vibrations of cyclohexanone

For the assignment of CH_2 group frequencies, basically six fundamentals can be associated to each CH_2 group namely CH_2 ass, CH_2 ss, CH_2 scissoring and CH_2 rocking which belongs to in-plane vibration and two out-of-plane vibrations viz. CH_2 wagging and CH_2 twisting modes and are expected to be depolarized [45]. The asymmetric CH_2 stretching vibrations are generally observed below 3000 cm^{-1}, while the symmetric stretch will appear between 3000–2800 cm^{-1} [46-48]. The vibrations belonging to cyclohexane ring, the stretching region corresponding to CH_2 asymmetric and symmetric stretching vibrations are observed separately both in IR and in Raman as strong and medium intense bands at 3007 and 3015, 2775 cm^{-1} respectively. We assigned that this band is obtained at 2907, 2870, 2766, 2753 and 2998, 2930, 2806, 2776 cm^{-1}in HF and DFT methods, respectively. They are very pure modes since their PED contributions are above 97%. The spectral distinction between CH_2 groups involving C2 and that involving C1 and C3 can be observed for bending vibrations. The scissoring vibrations involving C2 and C3 can be observed in IR band at 1411 cm^{-1} and weak Raman band at 1415 cm^{-1} respectively. The CH_2 scissoring modes were observed at 1432, 1420 and 1407 cm^{-1} in DFT method. The band at 1179 cm^{-1}in FT-IR and 1188cm^{-1} in FT-Raman is assigned to CH_2 rocking vibration. The CH_2 twisting vibrations are observed at 1138 cm^{-1} in FT-IR and 1146 cm^{-1} in FT-Raman. The bands observed at 566 cm^{-1} in FT-IR and 990, 833, 563 cm^{-1} in FT-Raman spectra are assigned to CH_2 wagging vibration

4.7.6 Ring vibrations

In case of 1A4MP, the carbon atoms coupled together in the hexagonal chain of ring possesses two C–C stretching vibrations at 848 and 896 cm^{-1} in FT-IR and FT-Raman. The inplane and out-of-plane bending vibrations of the benzene ring are generally observed below 1000 cm^{-1} [49] and these modes are not pure but they contribute drastically from other vibrations and are substituent-sensitive. In the title molecule, the ring in-plane (δ_{ring}) and out-of plane (γ_{ring}) bending modes are affected to a great extent by the substituents and produce bands below 600 cm^{-1}. From PED results, the bands present at 474 cm^{-1} in FT-Raman and FT-IR spectra are assigned to γ_{ring}. The scaled theoretical wavenumbers corresponding to all the ring vibrations are found to have a good correlation with their available experimental observations.

4.7.7 UV–VIS spectra analysis

Molecules allow strong π–π* and σ –σ* transition in the UV-Vis region with high extinction coefficients. Ultraviolet spectra analyses of 1A4MP have been researched by theoretical calculation. In order to understand electronic transitions of compound, TD-DFT calculations on electronic absorption spectra in gas phase and solvent (Dimethyl sulfoxide and acetone) were performed. The calculated frontier orbital energies, absorption wavelengths (λ), oscillator strengths (*f*) and excitation energies (*E*) for gas and solvent (Dimethyl sulfoxide and acetone) phase are illustrated in Table 9 and the UV-Vis spectra of 1A4MPis shown in Fig. 7. Calculations of molecular orbital geometry show that the visible absorption maxima of this molecule correspond to the electron transition between frontier orbitals. As can be seen from Table 9, the calculated absorption maximum values have been found to be 365.58, 327.27, 319.43 nm for gas phase, 348.31, 322.65, 303.82 nm for dimethyl sulfoxide solution and 348.58, 322.43, 304.7 nm for acetone solution at DFT/B3LYP/6–311+G(d,p) method.

4.8 Conclusion

The FT-IR and FT-Raman spectra were recorded and detailed vibrational assignments for 1A4MP has been proposed, aided by the hybrid HF and density functional method (B3LYP) using 6–311+G(d,p) basis sets. The bond lengths and bond angles are found to be almost basis set independent. The PED contribution revealed that, C–N and N–N stretching vibrations are highly coupled with each other, since the experimental frequency values are less than the literature value. The mapped isodensity surfaces for the frontier molecular orbitals were plotted. The smallest energy gap (HOMO–LUMO = –4.09858eV) between HOMO and LUMO orbitals revealed that the molecule used in this study belongs to soft material and charge transfer interactions takes place

within the molecule, which is responsible for bioactive property of the biomedical compound. The NBO analysis confirms the hyper conjugation interaction. In addition, the nucleophilic and electrophilic sites on the MEP surface were determined. The charges accumulated on various constituents of MEP surface were reported along with their electric potential values. The detailed descriptions for the vibrational normal modes of 1A4MP were presented on the basis of combined experimental and theoretical IR and Raman studies.

Reference

[1] C. James, A. Amal Raj, R. Reghunathan, V.S. Jayakumar, I. Hubert Joe, *J. Raman Spectrosc.* **37** (2006) 1381–1392.

[2] M. Enrique, Cabaleiro-Lago, M.A. Rios*, J. Chem. Phys.* **113** (2000) 9523–9531.

[3] M.J. Frisch, G.W. Trucks, H.B. Schlegel, G.E. Scuseria, M.A. Robb, J.R. Cheeseman, G. Scalmani, V. Barone, B. Mennucci, G.A. Petersson, H. Nakatsuji, M. Caricato, X. Li, H. P. Hratchian, A.F. Izmaylov, J. Bloino, G. Zheng, J.L. Sonnenberg, M. Hada, M. Ehara, K. Toyota, R. Fukuda, J. Hasegawa, M. Ishida, T. Nakajima, Y. Honda, O. Kitao, H. Nakai, T. Vreven, J. A. Montgomery, Jr., J. E. Peralta, F. Ogliaro, M. Bearpark, J.J. Heyd, E. Brothers, K. N. Kudin, V. N. Staroverov, R. Kobayashi, J. Normand, K. Raghavachari, A.Rendell, J. C. Burant, S.S. Iyengar, J. Tomasi, M. Cossi, N. Rega, J.M. Millam, M. Klene, J.E. Knox, J.B. Cross, V. Bakken, C.Adamo, J. Jaramillo, R. Gomperts, R.E. Stratmann, O. Yazyev, A.J. Austin, R. Cammi, C. Pomelli, J.W. Ochterski, R.L. Martin, K. Morokuma, V.G. Zakrzewski, G. A. Voth, P. Salvador, J.J. Dannenberg, S. Dapprich, A.D. Daniels, O. Farkas, J.B. Foresman, J.V. Ortiz, J. Cioslowski, D.J. Fox, Gaussian, Inc., Wallingford CT, (2009).

[4] A.D. Becke, *J. Chem. Phys.* **98** (1993) 5648–5652.

[5] C. Lee, W. Yang, R.C. Parr, *J. Phys. Rev.* **B 37 (**1998) 785–789.

[6] G. Rauhut, P. Pulay, *J. Phys. Chem.* **99** (1995) 3093–3100.

[7] P. Pulay, G. Fogarasi, G. Pongor, J.E. Boggs, A. Vargha, *J. Am. Chem. Soc*. **105** (1983) 7037–7047.

[8] G. Fogarasi, X. Zhou, P.W. Taylor, P. Pulay*, J. Am. Chem. Soc.* **114** (1992) 8191– 8201.

[9] T. Sundius, J. Vib. Spectrosc. **29** (2002) 89–95.

[10] MOLVIB: *A Program for Harmonic Force Field Calculations,* QCPE Program No. **807** (2002).

[11] P. Pulay, G. Fogarasi, F. Pong, J.E. Boggs, *J. Am. Chem. Soc.* **101 (**1979) 2550.

[12] A.E. Reed, F. Weinhold*, J. Chem. Phys.* **83** (1985) 1736–1740.

[13] M. Snehalatha, C. Ravikumar, I. Hubert Joe, V.S. Jayakumar, *J. Raman Spectrosc.* **40** (2009) 1121–1126.

[14] I. Hubert Joe, Irena. Kostova, C. Ravikumar, M. Amalanathan, Simona. CintaPinzaru, *J. Raman Spectrosc***. 40 (**2009) 1033–1038.

[15] A.E. Ledesma, J. Zinczuk, A. Ben Altabef, J.J. Lopez Gonzalez, S.A. Brandan, *J. Raman Spectrosc.* **40** (2009) 1004–1010.
[16] J. Chocholoussova, V. Vladimir Spirko, P. Hobza*, J. Phys. Chem. Phys*. **6** (2004) 37–41.
[17] Y.F. Li, W.M. Wang, *Acta. Cryst.* **E67** (2011) o2453-o2459.
[18] D. Sajan, K. Udaya Lakshmi, Y. Erdogdu, I. Hubert Joe, *Spectrochim .Acta.* **A78** (2011) 113-121.
[19] C. Jesintha John, M. Amalanathan, A.R. Twinkle, P. Srinivasan, I. Hubert Joe, *Spectrochim. Acta*. **A81** (2011) 151-161.
[20] R. Zhang, B. Dub, G. Sun, Y. Sun, *Spectrochim. Acta.* **A75** (2010) 1115–1124.
[21] S. Yazici, C. Albayrak, I. Gumrukcuoglu, .Senel, O. Buyukgungor*, J. Mol. Struct.* **985** (2011) 292–298.
[22] B. Kosar, C. Albayrak, *Spectrochim. Acta.* **A78** (2011) 160–167.
[23] A.M. Asiri, M. Karabacak M. Kurt, K.A. Alamry, *Spectrochim. Acta.* **A82** (2011) 444–455.
[24] N. Sundaraganesan, J. Karpagam, S. Sebastian, J.P. Cornard, *Spectrochim. Acta.* **A73** (2009) 11–19.
[25] D.M. Burland, R.D. Miller, C.A. Walsh, *Chem. Rev*. **94** (1994) 31-74.
[26] D.A. Kleinmen, Phys.Rev.**126** (1962) 1977-1979.
[27] B. Edwin, M. Amalanathan, I. Hubert Joe, *Spectrochimic. Acta A*. **96** (2012) 10–17.
[28] R.S. Mulliken*, J. Chem. Phys.* **23** (1955) 1833–1840.
[29] J.S. Murray, K. Sen, *Molecular Electrostatic Potentials, Concepts and Applications, Elsevier,* Amsterdam, (1996).
[30] E. Scrocco, J. Tomasi, in: P. Lowdin (Ed.) *Advances in Quantum Chemistry,* Academic Press, New York, (1978).
[31] N.B. Colthup, L.H. Daly, S.E. Wiberley, *Introduction to Infrared and Raman Spectroscopy*, Academic Press, New York, (1990).
[32] A.D. Becke, *J. Chem. Phys.* **98** (1993) 5648–5652.
[33] L.J. Bellamy, *The Infrared Spectra of Complex Molecules* vol.2, Chapman and Hall, London, (1980).
[34] M. Karabacak, M. Cinar, *Spectrochim. Acta.* **A86** (2012) 590–599.
[35] N.B. Colthup, L.H. Daly, S.E. Wiberley, *Introduction to Infrared and Raman Spectroscopy*, Academic Press, New York, (1990).
[36] V. Krishnakumar, R. Ramasamy, *Spectrochim. Acta*. **A61** (2005) 2526–2532.
[37] M. Silverstein, G. Clayton Basseler, C. Morill, *Spectrometric Identification of Organic Compounds,* Wiley, New York, (1981).
[38] S.F. Parker, *Spectrochim. Acta*. **A51** (1995) 2067
[39] B. Smith, Infrared Spectral Interpretation, A Systematic Approach, CRC Press, New York, DC, (1999).
[40] N.B. Colthup, L.H. Daly, S.E. Wiberley, *Introduction to Infrared and Raman Spectroscopy,* 3rd ed., Academic Press New York, (1990).

[41] Y. Huang, D.F.R. Gilson, I.S. Butler, *J. Chem. Phys.* **97** (1993) 1998–2001.
[42] M. Gussoni, C. Castiglioni, M.N. Ramos, M.C. Rui, G. Zerbi, *J. Mol. Struct.* **224** (1990) 445–470.
[43] V. Hernandz, C. Castiglioni, G. Zerbi*, J. Mol. Struct.* 324 (1994) 189–198.
[44] R. Shanker, R.A. Yadav, I.S. Singh, O.N. Singh, *Indian J. Pure Appl. Phys.* **23 (**1985) 339
[45] G. Varsanyi, *Vibrational Spectra of Benzene Derivatives,* Academic Press, New York (1969).
[46] G. Litivinov, Proceedings of the XIII *International Conference on Raman Spectroscopy*, Wurzburg, Germany, (1992).
[47] K. Furie, V. Mohacek, M. Bonifacic, I. Stefanic, *J. Mol. Struct.* **267** (1992) 39–44.
[48] V. Balachandran, G. Mahalakshmi, A. Lakshmi, A. Janaki*' Spectrochim. Acta.* **97** (2012) 1101-1110.
[49] S. Gunasekaran, R.A. Balaji, S. Kumaresan, G. Anand, S. Srinivasan, Can*. J. Anal. Sci. Spectrosc.* **53** (2008) 149–162.

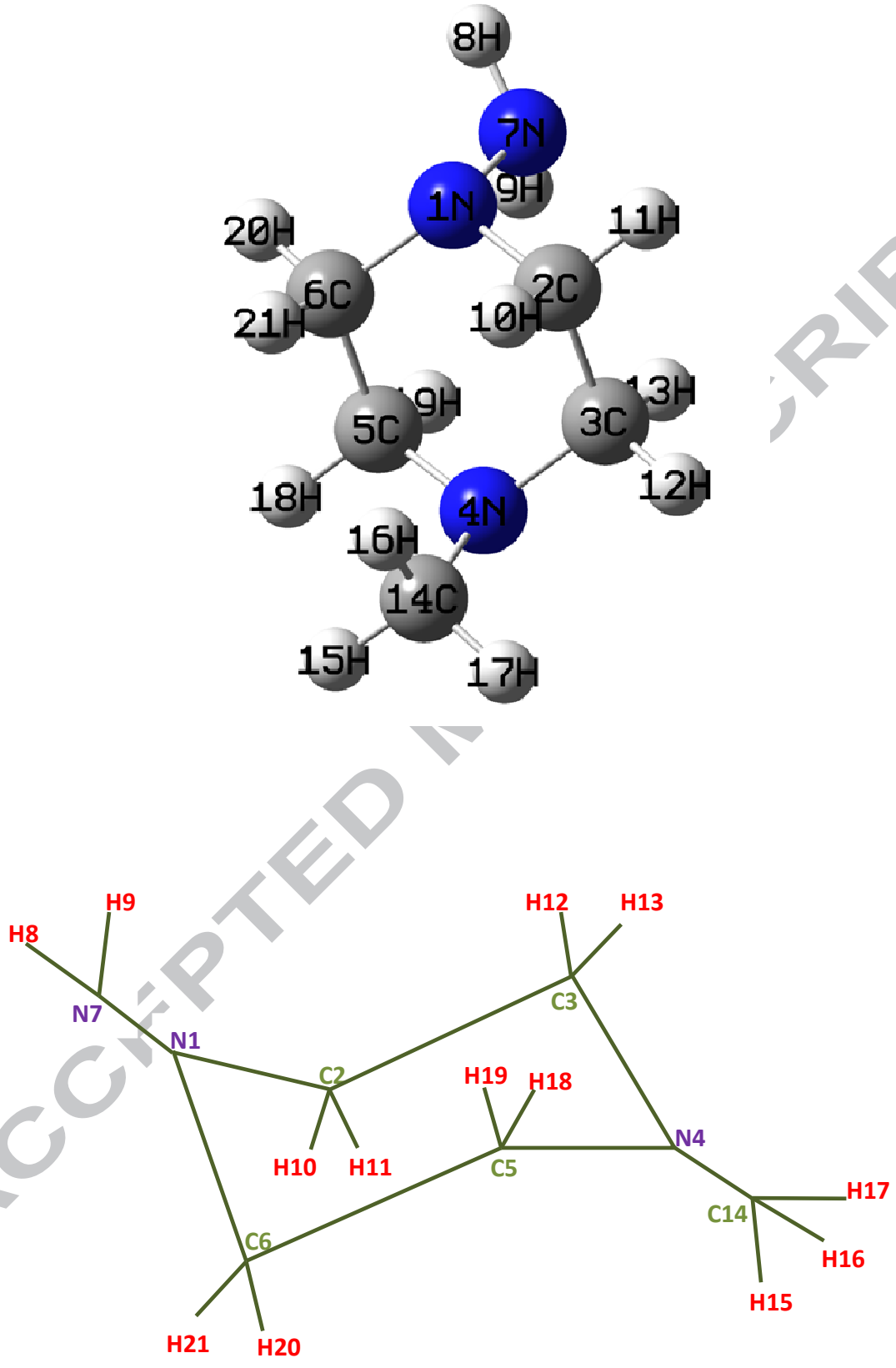

Fig. 1

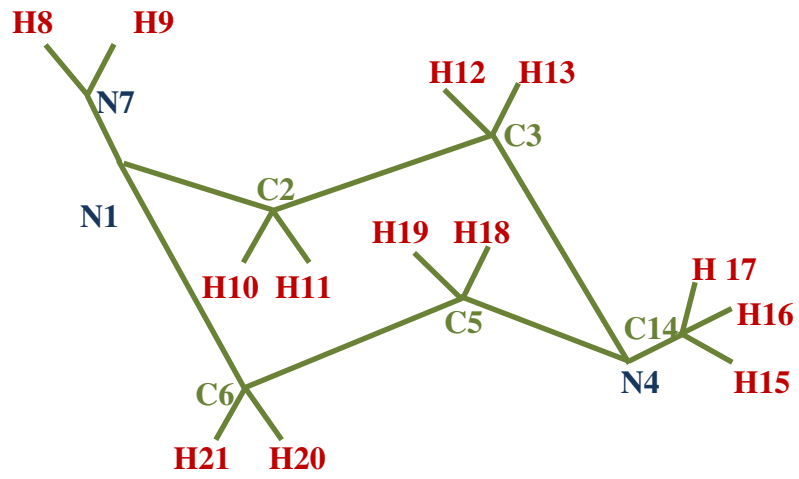

cis - cis(I)

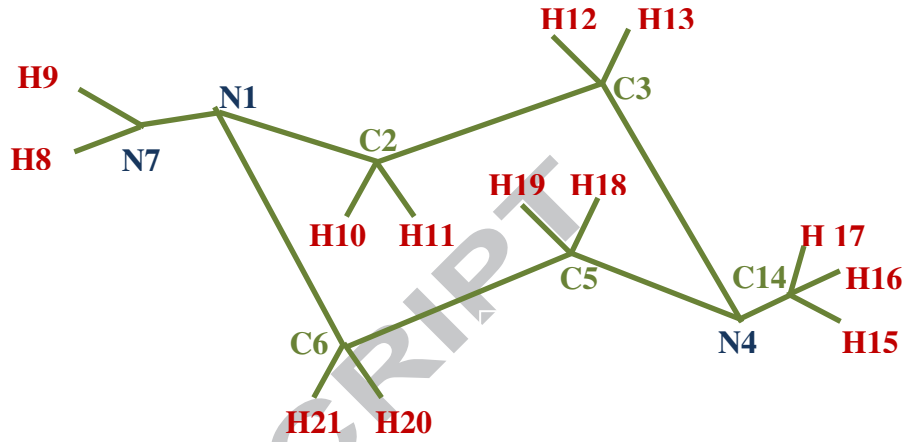

trans - cis(III)

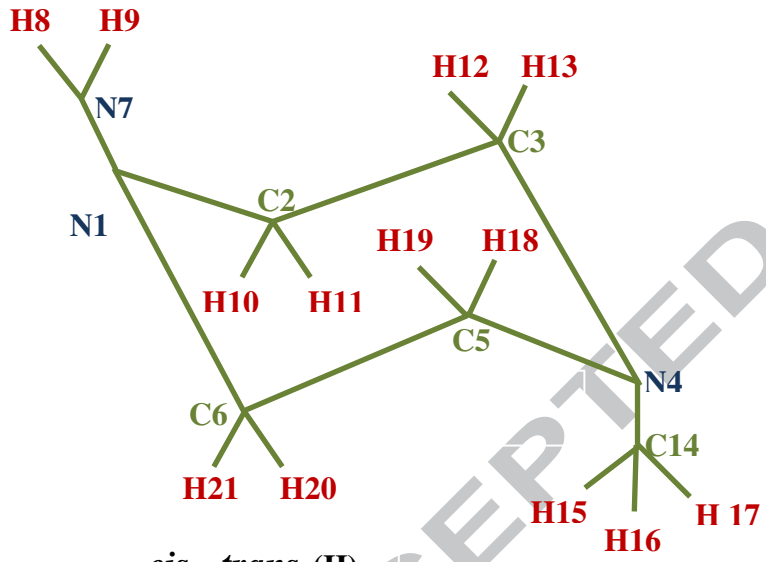

cis - trans (II)

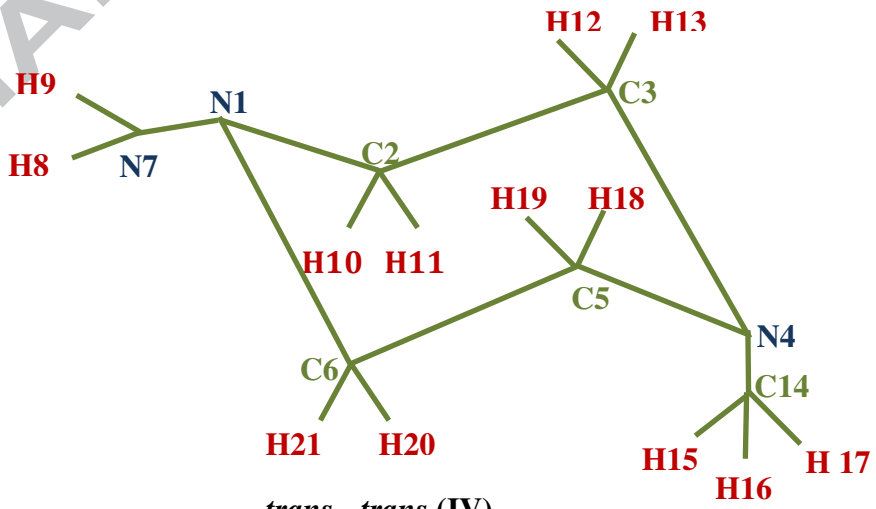

trans - trans (IV)

Fig. 2

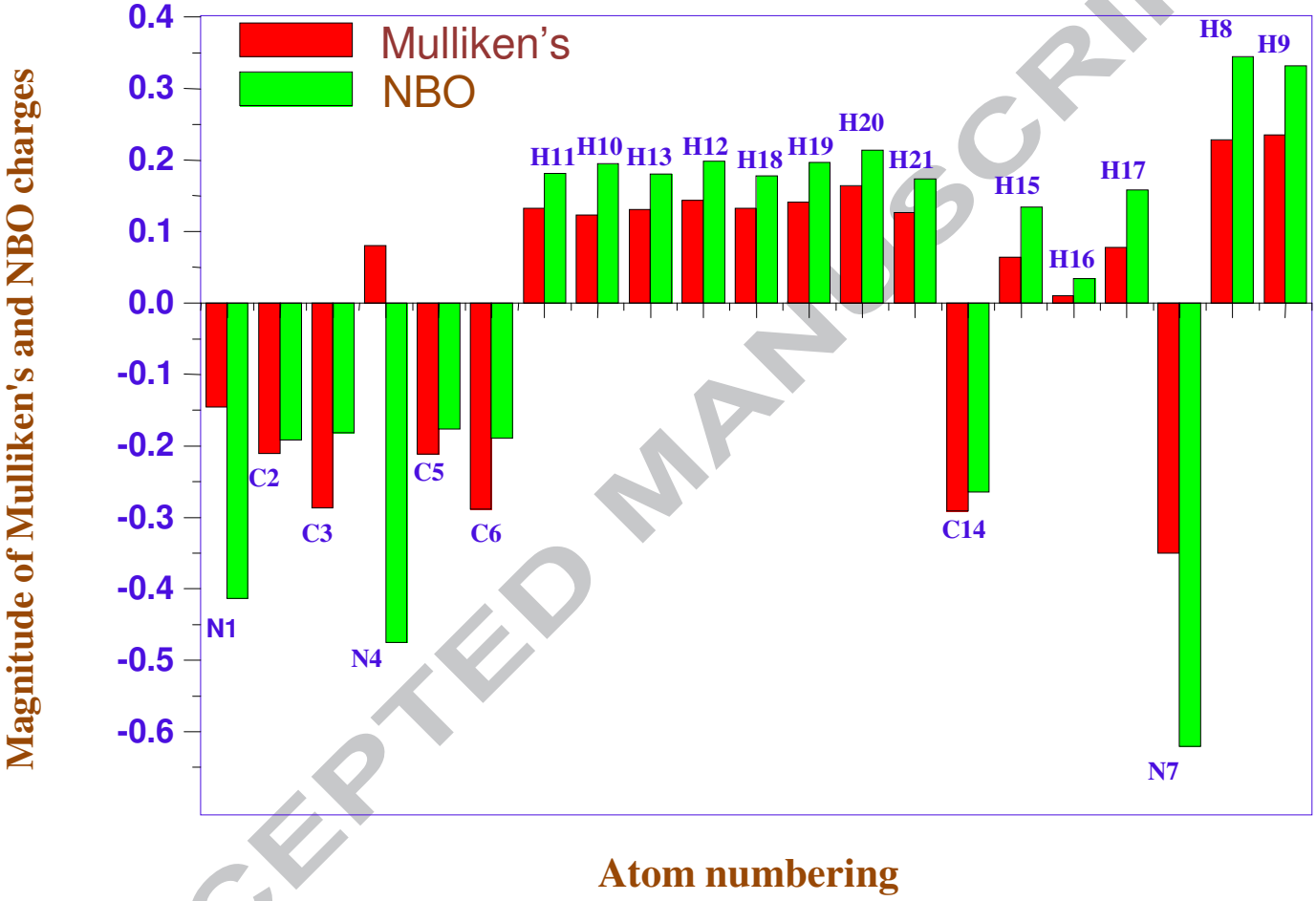

Fig. 3

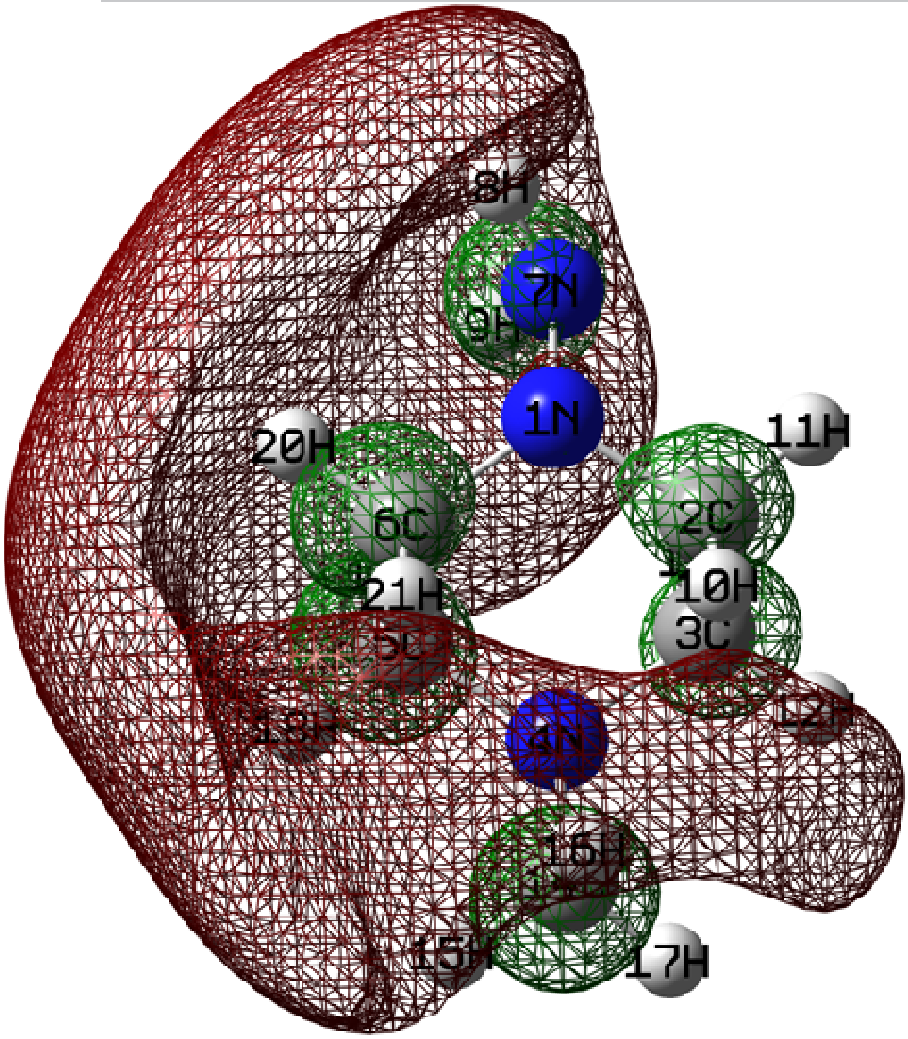

LUMO
(Excited State)

E_{LUMO}= -0.1540eV

$\Delta E_{HOMO-LUMO}$= -4.09858eV

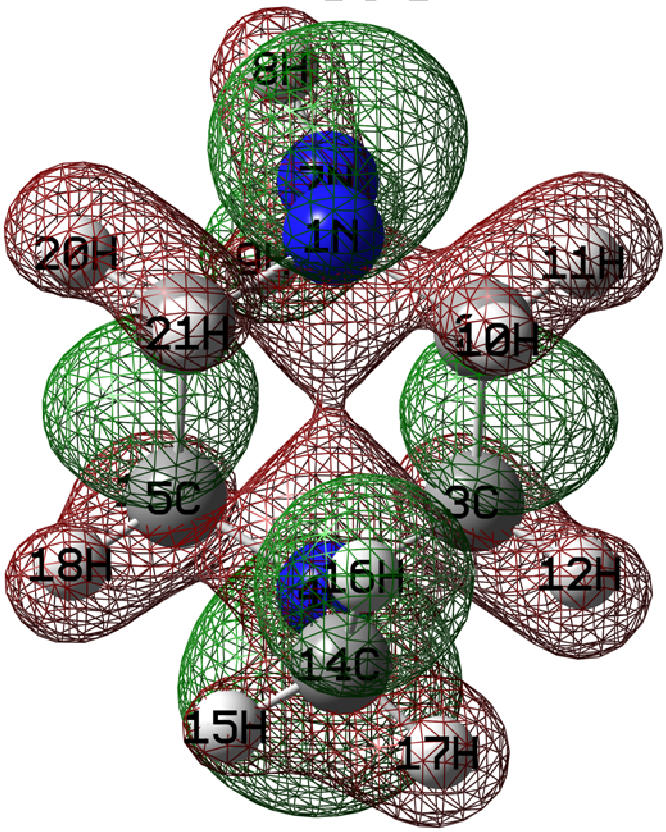

HOMO
(Ground State)

E_{HOMO}= -4.2526eV

Fig. 4

	V(r)	Point Charges (e)
7N	−0.9749	−18.3752
2C	−0.3183	−14.7439
16H	−0.2091	−1.19416
6C	−0.1213	−14.7498
15H	−0.0765	−1.15066
13H	−0.0492	−1.11266
5C	−0.0395	−14.7503
17H	−0.0318	−1.13896
14C	−0.0181	−14.8268
18H	−0.0072	−1.11658
21H	−0.0041	−1.11736
9H	0.381165	−1.06106
8H	0.370941	−1.04697
1N	0.364936	−18.3861
4N	0.360162	−18.4490
10H	0.087325	−1.10310
11H	0.075592	−1.11116
20H	0.069890	−1.11359
12H	0.052168	−1.10818
19H	0.045967	−1.10889
3C	0.042440	−14.7477

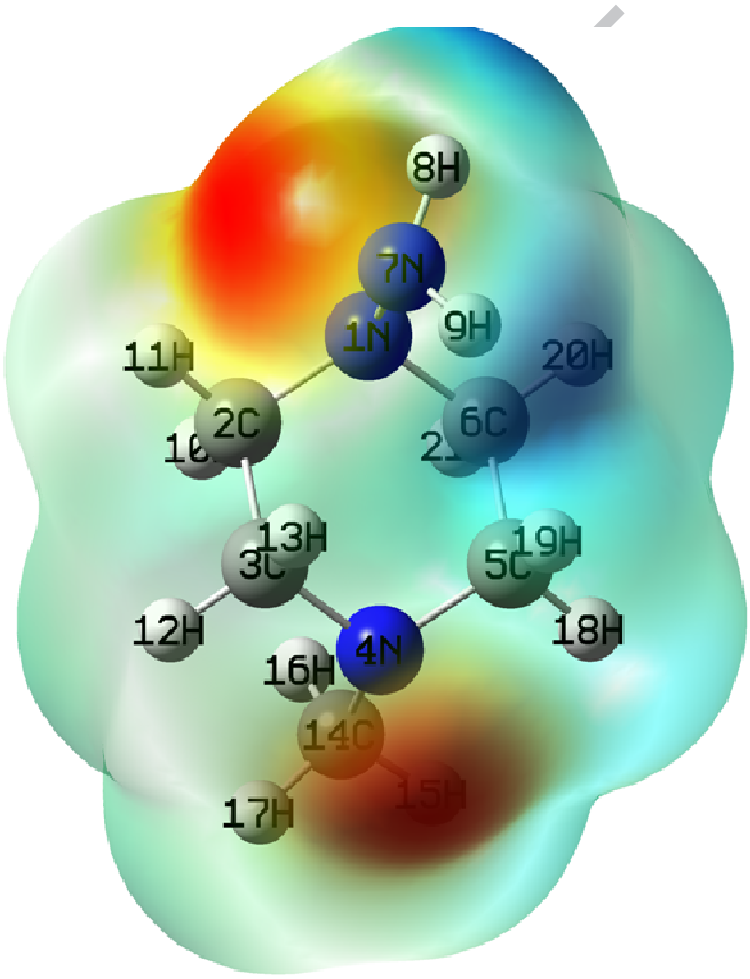

Fig. 5

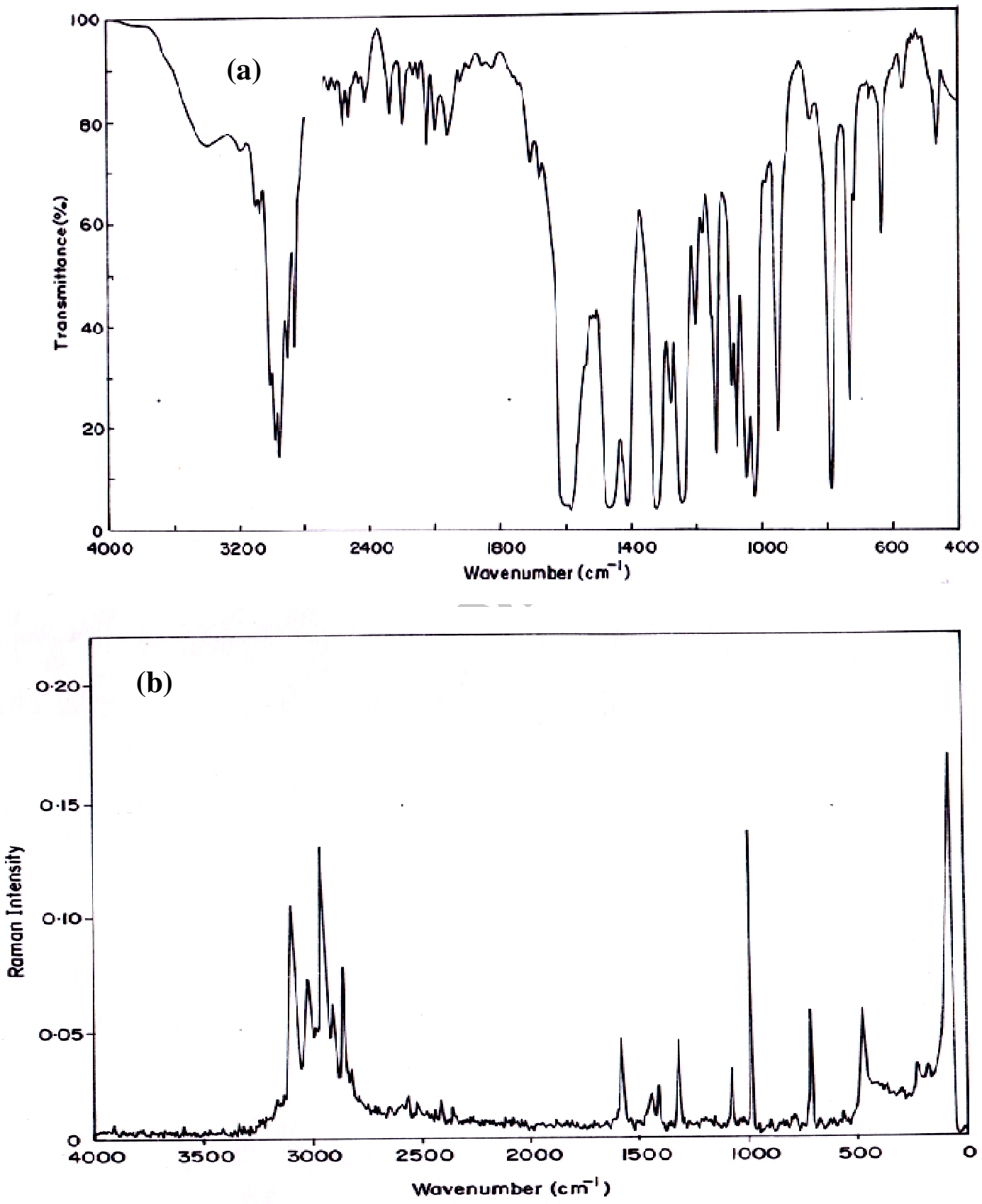

Fig. 6

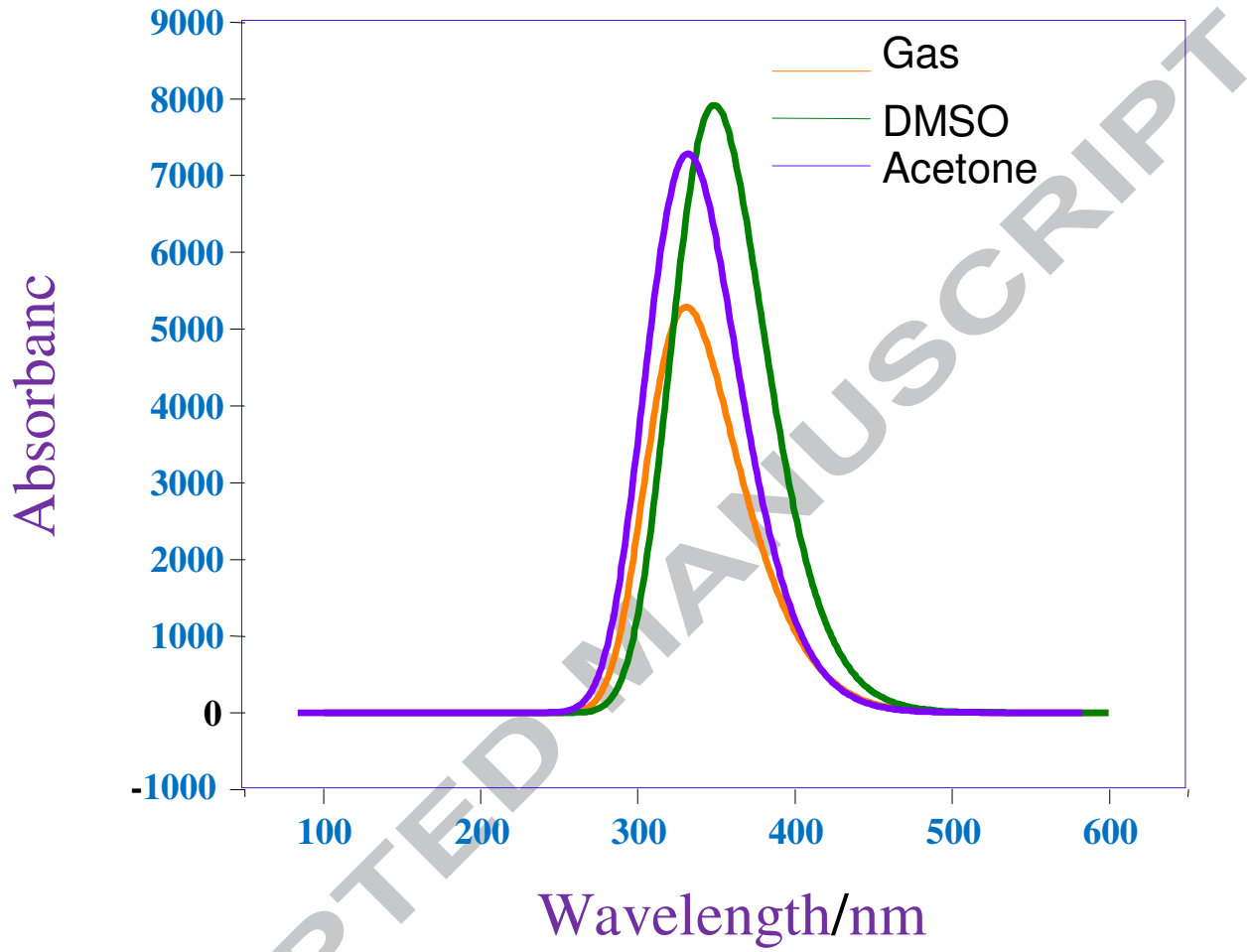

Fig. 7

FIGURE CAPTIONS

Fig. 1 Optimized molecular structure of 1-Amino-4-methylpiperazine

Fig. 2 Possible conformers of 1-Amino-4-methylpiperazine

Fig. 3 Comparative graph of Mulliken's vs. natural atomic charges.

Fig. 4 The frontier molecular orbitals and related energies (in gas phase).

Fig. 5 Molecular electrostatic potential (MEP) surface map for 1-Amino-4-methylpiperazine

Fig. 6 (a) FT-IR and (b) FT-Raman spectrum of 1-Amino-4-methylpiperazine

Fig. 7 UV-VIS spectra of 1-Amino-4-methylpiperazine in gas, DMSO and acetone

TABLE 1
Definition of internal symmetry coordinates of 1A4MP

No.	Symbols	Type	Definition
Stretching			
1–8	R_i	C–$H_{(aromatic)}$	C2–H10,C2–H11,C3–H13,C3–H12,C5–H18,C5–H19,C6–H20,C6–H21
9–13	R_i	C–N	C2–N1,C6–N1,C3–N4,C5–N4,C14–N4
14–15	R_i	C–C	C5–C6,C2–C3
16–18	R_i	C–$H_{(methyl)}$	C14–H15,C14–H16,C14–H17
19	R_i	N–N	N1–N7
20–21	R_i	N–H	N7–H8,N7–H9
Bending			
22–27	α_i	Ring	N1–C2–C3,C2–C3–N4,C3–N4–C5,N4–C5–C6,C5–C6–N1,C6–N1–C2
28–43	α_i	$NCH_{(amide)}$	N4–C3–H13,N4–C3–H12,C2–C3–H13,C2–C3–H12
		$CCH_{(aromatic)}$	C3–C2–H11,C3–C2–H10,N1–C2–H11,N1–C2–H10
		$CCH_{(ethyl)}$	N4–C5–H18,C6–C5–H18,N4–C5–H19,C6–C5–H19, C5–C6–H20,H13–C6–N1,C5–C6–H21,N1–C6–H21
44–47	α_i	CNC	C3–N4–C14,C5–N4–C14,
		CNN	C2–N1–N7,C6–N1–N7
48–50	α_i	$NNH_{(amide)}$	N1–N7–H9,N1–N7–H8,
		HNH	H13–N7–H8
51–56	α_i	$NCH_{(methyl)}$	N4–C14–H15,N4–C14–H16,N4–C14–H17
		HCH	H16–C14–H15,H16–C14–H17,H17–C14–H15
Out–of–plane bending			
57–58	ω_i	C–N	C3–N4–C14–C5,C6–N1–N7–C2
Torsion			
59–64	τ_{ring}	Ring	N1–C2–C3–N4,C2–C3–N4–C5,C3–N4–C5–C6,N4–C5–C6–N1,C5–C6–N1–C2,C6–N1–C2–C3
64–67	τ_i	t(N)–CH3	(C5,C6)–N4–C14–(H15,H16,H17)
68–69	τ_i	CNNH	(C2,C6)–N1–N7–(H13,H12)

TABLE 2
Definition of local symmetry coordinates of 1A4MP

No.	Symbol	Definition
Stretching		
1–4	$CH_{2(aromatic)ss}$	$(R_1+R_2)/\sqrt{2},(R_3+R_4)/\sqrt{2},(R_5+R_6)/\sqrt{2},(R_7+R_8)/\sqrt{2}$
5–8	$CH_{2(aromatic)ass}$	$(R_1-R_2)/\sqrt{2}-(R_3-R_4)/\sqrt{2}-(R_5-R_6)/\sqrt{2}-(R_7-R_8)/\sqrt{2}$
9–13	CN	$R_9,R_{10},R_{11},R_{12},R_{13}$
14–15	CC	R_{14},R_{15}
16	CH_{3ss}	$(R_{16}+R_{17}+R_{18})/\sqrt{3}$
17	CH_{3ips}	$(2R_{16}-R_{17}-R_{18})/\sqrt{6}$
18	CH_{3ops}	$(R_{17}-R_{18})/\sqrt{2}$
19	NN	R_{19}
20	$NH_{2(amide)ss}$	$(R_{15}+R_{16})/\sqrt{2}$
21	$NH_{2(amide)ass}$	$(R_{15}-R_{16})/\sqrt{2}$
Bending		
22	R_{trigd}	$(\alpha_{22}-\alpha_{23}+\alpha_{24}-\alpha_{25}+\alpha_{26}-\alpha_{27})/\sqrt{6}$
23	R_{symd}	$(-\alpha_{22}-\alpha_{23}+2\alpha_{24}-\alpha_{25}+\alpha_{26}-\alpha_{27})/\sqrt{12}$
24	R_{asymd}	$(\alpha_{22}-\alpha_{23}+\alpha_{25}-\alpha_{26})/\sqrt{2}$
25–28	$CH_{2(aromatic)sciss}$	$\alpha_{28}+\alpha_{29}+\alpha_{30}+\alpha_{31},\alpha_{32}+\alpha_{33}+\alpha_{34}+\alpha_{35},\alpha_{36}+\alpha_{37}+\alpha_{38}+\alpha_{39},\alpha_{40}+\alpha_{41}+\alpha_{42}+\alpha_{43}$
29–32	$CH_{2(aromatic)wag}$	$\alpha_{28}-\alpha_{29}+\alpha_{30}-\alpha_{31},\alpha_{32}-\alpha_{33}+\alpha_{34}-\alpha_{35},\alpha_{36}-\alpha_{37}+\alpha_{38}+\alpha_{39},\alpha_{40}-\alpha_{41}+\alpha_{42}-\alpha_{43}$
33–36	$CH_{2(aromatic)rock}$	$\alpha_{28}+\alpha_{29}-\alpha_{30}-\alpha_{31},\alpha_{32}+\alpha_{33}-\alpha_{34}-\alpha_{35},\alpha_{36}+\alpha_{37}-\alpha_{38}-\alpha_{39},\alpha_{40}+\alpha_{41}-\alpha_{42}-\alpha_{43}$
37–40	$CH_{2(aromatic)twist}$	$\alpha_{28}-\alpha_{29}-\alpha_{30}+\alpha_{31},\alpha_{32}-\alpha_{33}-\alpha_{34}+\alpha_{35},\alpha_{36}-\alpha_{37}-\alpha_{38}+\alpha_{39},\alpha_{40}-\alpha_{41}-\alpha_{42}+\alpha_{43}$
41	CNC	$(\alpha_{44}-\alpha_{45})/\sqrt{6}$
42	CNN	$(\alpha_{46}-\alpha_{47})/\sqrt{6}$
43	NH_{2sciss}	$(2\alpha_{50}-\alpha_{48}-\alpha_{49})/\sqrt{6}$
44	NH_{2rock}	$(\alpha_{48}-\alpha_{49})/\sqrt{2}$
45	NH_{2twist}	$(\alpha_{48}+\alpha_{49})/\sqrt{2}$
46	CH_{3sb}	$(-\alpha_{51}-\alpha_{52}-\alpha_{53}+\alpha_{54}+\alpha_{55}+\alpha_{56})/\sqrt{6}$
47	CH_{3ipb}	$(-\alpha_{54}-\alpha_{55}-2\alpha_{56})/\sqrt{6}$
48	CH_{3opb}	$(\alpha_{54}-\alpha_{56})/\sqrt{2}$
49	CH_{3ipr}	$(2\alpha_{52}-\alpha_{51}-\alpha_{53})/\sqrt{6}$
50	CH_{3opr}	$(\alpha_{451}-\alpha_{56})/\sqrt{6}$
51–52	ωCN	ω_{57},ω_{58}
53	tRing	$(\tau_{59}-\tau_{60}+\tau_{61}-\tau_{62}+\tau_{63}-\tau_{64})/\sqrt{6}$
54	tR_{sym}	$(\tau_{59}-\tau_{61}+\tau_{62}-\tau_{64})/\sqrt{2}$
55	tR_{asym}	$(-\tau_{59}+2\tau_{60}-\tau_{61}-\tau_{62}+2\tau_{63}-\tau_{64})/\sqrt{2}$
56	tCH_3	$(\tau_{65}+\tau_{66}+\tau_{67})/\sqrt{3}$
57	tNH_2	$(\tau_{68}+\tau_{69})$

TABLE 3

Optimized geometrical parameters of 1A4MP bond length (Å), angle(^{0}) and dihedral angle(^{0}) by HF and B3LYP methods of 6−311+G(d,P) basis set

Bond	Value(Å)				Value(^{0})				Value(^{0})	
length	a	b	Exp[c]	Bond angles	a	b	Exp[c]	Dihedral angles	a	b
N1−C2	1.47	1.46	1.45	C2−N1−C6	110.36	109.97	112.64	C6−N1−C2−C3	−51.99	−51.96
N1−C6	1.47	1.45	1.45	C2−N1−N7	114.59	114.50	-	C6−N1−C2−H11	68.03	68.07
N1−N7	1.43	1.41	-	C6−N1−N7	111.13	110.66	-	C6−N1−C2−H10	−175.55	−175.43
C2−C3	1.53	1.53	1.51	N1−C2−C3	113.47	113.49	110.30	N7−N1−C2−C3	73.32	74.38
C2−H11	1.09	1.09	0.97	N1−C2−H11	107.59	107.38	109.60	N7−N1−C2−H11	−166.66	−165.59
C2−H10	1.09	1.09	0.97	N1−C2−H10	108.86	108.65	109.60	N7−N1−C2−H10	−50.24	−49.09
C3−N4	1.46	1.45	1.44	C3−C2−H11	108.49	108.60	109.60	C2−N1−C6−C5	51.89	52.27
C3−H13	1.11	1.10	0.97	C3−C2−H10	110.48	110.66	109.60	C2−N1−C6−H20	174.83	175.20
C3−H12	1.09	1.09	0.97	H11−C2−H10	107.75	107.87	108.10	C2−N1−C6−H21	−68.28	−67.74
N4−C5	1.46	1.45	1.44	C2−C3−N4	110.36	110.29	111.00	N7−N1−C6−C5	−75.59	−75.99
N4−C14	1.45	1.44	1.47	C2−C3−H13	110.58	110.43	109.40	N7−N1−C6−H20	47.35	46.94
C5−C6	1.53	1.53	1.50	C2−C3−H12	109.09	109.48	109.40	N7−N1−C6−H21	164.24	164.00
C5−H18	1.11	1.10	0.97	N4−C3−H13	111.13	111.10	109.40	C2−N1−N7−H8	84.71	85.23
C5−H19	1.09	1.09	0.97	N4−C3−H12	109.03	108.94	109.40	C2−N1−N7−H9	−34.55	−35.23
C6−H20	1.09	1.08	0.97	H13−C3−H12	106.56	106.50	108.00	C6−N1−N7−H8	−150.33	−148.82
C6−H21	1.10	1.09	0.97	C3−N4−C5	111.34	110.98	109.60	C6−N1−N7−H9	90.40	90.72
C14−H15	1.09	1.09	0.96	C3−N4−C14	112.25	112.03	111.60	N1−C2−C3−N4	55.33	54.53
C14−H16	1.11	1.10	0.96	C5−N4−C14	112.37	112.06	110.50	N1−C2−C3−H13	−67.86	−68.84
C14−H17	1.09	1.08	0.96	N4−C5−C6	110.38	110.46	111.80	N1−C2−C3−H12	175.19	174.29
N7−H8	1.01	1.00	-	N4−C5−H18	111.29	111.22	109.30	H11−C2−C3−N4	−63.99	−64.99
N7−H9	1.02	1.00	-	N4−C5−H19	108.78	108.62	109.30	H11−C2−C3−H13	172.81	171.65
				C6−C5−H18	109.97	109.88	109.30	H11−C2−C3−H12	55.86	54.77
				C6−C5−H19	109.30	109.55	109.30	H12−C2−C3−N4	177.78	177.10
				H11−C5−H19	107.04	107.02	107.90	H12−C2−C3−H13	54.59	53.74
				N1−C6−C5	113.19	113.46	110.40	H12−C2−C3−H12	−62.37	−63.14
				N1−C6−H20	108.24	107.91	109.60	C2−C3−N4−C5	−57.08	−56.43
				N1−C6−H21	107.53	107.23	109.60	C2−C3−N4−C14	176.82	176.60
				C5−C6−H20	110.57	110.63	109.60	H13−C3−N4−C5	65.72	66.61
				C5−C6−H21	108.65	108.81	109.60	H13−C3−N4−C14	−60.38	−60.36
				H13−C6−H21	108.52	108.66	108.10	H12−C3−N4−C5	−177.25	−176.23
				N4−C14−H15	109.93	109.85	109.50	H12−C3−N4−C14	56.64	56.80
				N4−C14−H16	112.77	112.82	109.50	C3−N4−C5−C6	57.09	56.90
				N4−C14−H17	109.88	109.76	109.50	C3−N4−C5−H18	−65.21	−65.50
				H15−C14−H16	108.09	108.11	109.50	C3−N4−C5−H19	177.26	176.81
				H15−C14−H17	107.97	108.12	109.50	C14−N4−C5−C6	−176.83	−176.19
				H16−C14−H17	108.06	108.05	109.50	C14−N4−C5−H18	60.87	61.41
				N1−N7−H8	108.45	107.76	-	C14−N4−C5−H19	−56.65	−56.29
				N1−N7−H9	113.09	112.70	-	C3−N4−C14−H15	−57.78	−57.38
				20−N7−H9	108.56	108.16	-	C3−N4−C14−H16	62.92	63.31
								C3−N4−C14−H17	−176.53	−176.07
								C5−N4−C14−H15	176.72	176.20
								C5−N4−C14−H16	−62.59	−63.11
								C5−N4−C14−H17	57.97	57.51
								N4−C5−C6−N1	−55.18	−55.27
								N4−C5−C6−H20	−176.61	−176.90
								N4−C5−C6−H21	64.08	64.10
								H11−C5−C6−N1	67.90	67.91
								H11−C5−C6−H20	−53.53	−53.73
								H11−C5−C6−H21	−172.83	−172.73
								H12−C5−C6−1N	−174.8	−174.86
								H12−C5−C6−H20	63.77	63.51

H12−C5−C6−H21	−55.53	−55.49					

[a]CalculatedbyHF/6311+G(d,p)
[b]CalculatedbyB3LYP/6311+G(d,p)
[c]TakenfromRef[17]

TABLE 4

Calculated dipole moment, polarizabilities, first order and second order hyperpolarizabilities.

				β			
		αComponents	Values(a.u.)	Components	Values(a.u.)	γComponents	Values(a.u.)
μ_x	−0.955	α_{xx}	−53.05	β_{xxx}	−0.1255	γ_{xxxx}	−804.84
μ_y	−1.262	α_{yy}	−49.24	β_{yyy}	0.1402	γ_{yyyy}	−345.6
μ_z	0.769	α_{zz}	−53.34	β_{zzz}	1.1142	γ_{zzzz}	−189.27
μ	1.76	α_{xy}	−3.49	β_{xyy}	−0.1835	γ_{xxyy}	−193.07
		α_{xz}	0.3	β_{yxx}	−9.6428	γ_{xxzz}	−185.48
		α_{yz}	−1.78	β_{zxx}	5.0368	γ_{yyzz}	−95.02
		α_0	−51.8805	β_{xzz}	3.3708	Averageγ	−39.514xE−35e.s.u
		α	0.593xE−24e.s.u.	β_{yzz}	−3.1767		
				β_{zyy}	−3.8165		
				β_{total}	1.1448xE−35e.s.u		

TABLE 5

The second order perturbation energies E (2) (kcal /mol) corresponding to the most important charge transfer interactions (donor −acceptor) of 1A4MP by DFT method.

Donor NBO(i)	ED(i) (e)	Acceptor NBO(j)	ED(j) (e)	E(2) kcal/mol	E(j)−E(i) a.u.	F(i,j) a.u.
BD(1)C3−N4	1.9539	BD*(1)C2−H10	0.01899	1.3	1.05	0.03
		BD*(1)N4−C5	0.06118	0.96	1.04	0.03
		BD*(1)N4−C14	0.03347	12.44	2.01	0.14
		BD*(1)C5−H19	0.01393	1.62	1.06	0.04
		BD*(1)C14−H15	0.06379	4.01	1.13	0.06
		BD*(1)C14−H17	0.04999	5.87	1.13	0.07
BD(1)N4−C5	1.9545	BD*(1)C3−N4	0.06255	1.03	1.03	0.03
		BD*(1)C3−H12	0.01420	1.63	1.06	0.04
		BD*(1)N4−C14	0.03347	12.47	2.01	0.14
		BD*(1)C14−H15	0.06379	4.86	1.13	0.07
		BD*(1)C14−H17	0.04999	4.97	1.13	0.07
BD(1)N4−C14	1.9695	BD*(1)C3−N4	0.06255	10.19	1.54	0.11
		BD*(1)N4−C5	0.06118	10.21	1.54	0.11
		BD*(1)C14−H15	0.06379	2.68	1.64	0.06
		BD*(1)C14−H16	0.12058	2.00	1.64	0.05
		BD*(1)C14−H17	0.04999	2.78	1.64	0.06
BD(1)C14−H17	1.9453	BD*(1)C3−N4	0.06255	22.1	0.83	0.12
		BD*(1)N4−C5	0.06118	0.67	0.83	0.02
		BD*(1)N4−C14	0.03347	8.99	1.8	0.11
BD(1)C14−H16	0.1206	BD*(1)N4−C14	0.03347	2.03	0.88	0.14
LP(1)N1	1.8477	BD*(1)C2−C3	0.03280	7.16	0.62	0.06
		BD*(1)C2−H11	0.03549	6.41	0.6	0.06
		BD*(1)C5−C6	0.03185	6.85	0.62	0.06
		BD*(1)C6−H21	0.03756	6.4	0.6	0.06
		BD*(1)N7−H8	0.01312	2.83	0.68	0.04
		BD*(1)N7−H9	0.01939	6.96	0.68	0.06
n(1)N4	1.7298	BD*(1)C2−C3	0.03280	4.25	0.6	0.05
		BD*(1)C3−H13	0.02874	6.54	0.59	0.06
		BD*(1)C5−C6	0.03185	4	0.61	0.05

		BD*(1)C5–H18	0.03112	6.33	0.59	0.06
		BD*(1)C14–H15	0.06379	15.93	0.67	0.10
		BD*(1)C14–H16	0.12058	50.58	0.67	0.17
		BD*(1)C14–H17	0.04999	7.99	0.67	0.07
n(1)N7	1.9671	BD*(1)N1–C2	0.03439	8.11	0.76	0.07

[a] $E^{(2)}$ means energy of hyper conjugative interaction (stabilization energy).
[b] Energy difference between donor and acceptor i and j NBO orbitals.
[c] F(*i,j*) is the Fock matrix element between i and j NBO orbitals

TABLE 6
Natural bond orbital analysis of 1A4MP

ED (a.u)	Bond(A–B)	Energy (a.u)	ED_A(%)	ED_B(%)	NBO	S%		P%	
1.98460	BD(1)N1–C2	−0.7495	61.48	38.52	$0.7841(sp^{1.90})0.6207(sp^{3.35})$	34.50	22.95	65.46	76.92
1.98344	BD(1)N1–C6	−0.7463	61.90	38.10	$0.7868(sp^{1.84})0.6172(sp^{3.36})$	35.21	22.89	64.76	76.98
1.99276	BD(1)N1–N7	−0.8170	53.13	46.87	$0.7289(sp^{2.32})0.6846(sp^{2.82})$	30.11	26.12	69.83	73.77
1.95392	BD(1)C3–N4	−0.6836	37.01	62.99	$0.6084(sp^{3.35})0.7936(sp^{3.10})$	22.99	24.38	76.92	75.58
1.95453	BD(1)N4–C5	−0.6823	63.19	36.81	$0.7949(sp^{3.08})0.6067(sp^{3.37})$	24.52	22.87	75.44	77.04
1.84766	L(1)N1	−0.2322			$(sp^{99.99})$	0.05		99.95	
1.72982	L(1)N4	−0.2168			$(sp^{99.99})$	0.06		99.89	
1.96706	L(1)N7	−0.3351			$(sp^{3.98})$	20.06		79.9	
0.03439	BD*(1)N1–C2	0.3278	38.52	61.48	$0.6207(sp^{1.90})-0.7841(sp^{3.35})$	34.50	22.95	65.46	76.92
0.02810	BD*(1)N1–C6	0.3857	38.10	61.90	$0.6172(sp^{1.84})-0.7868(sp^{3.36})$	35.21	22.89	64.76	76.98
0.02547	BD*(1)N1–N7	0.3691	46.87	6.12	$0.6846(sp^{2.32})-0.7289(sp^{2.82})$	30.11	26.12	69.83	73.77
0.03280	BD*(1)C2–C3	0.3680	50.21	49.79	$0.7086(sp^{2.46})-0.7056(sp^{2.36})$	28.92	29.75	71.03	70.21
0.06255	BD*(1)C3–N4	0.3753	62.99	37.01	$0.7936(sp^{3.35})-0.6084(sp^{.10})$	22.99	24.38	76.92	75.58
0.06118	BD*(1)N4–C5	0.3924	36.81	63.19	$0.6067(sp^{3.08})-0.7949(sp^{3.37})$	24.52	22.87	75.44	77.04
0.03185	BD*(1)C5–C6	0.3764	49.64	50.36	$0.7046(sp^{2.35})-0.7096(sp^{.42})$	29.83	29.18	70.13	70.77

TABLE 7
The charge distribution calculated by the Mulliken and natural bond orbital (NBO) methods.

Atoms	Atomiccharges (Mulliken)	Naturalcharges (NBO)
N1	−0.145301	−0.41357
C2	−0.210787	−0.19225
C3	−0.286809	−0.18194
N4	0.079900	−0.47545
C5	−0.212314	−0.17684
C6	−0.289258	−0.18938
N7	−0.350035	−0.62086
H8	0.132326	0.18076
H9	0.122921	0.19409
H10	0.130965	0.17994
H11	0.143602	0.19776
H12	0.131720	0.17740
H13	0.140867	0.19601
C14	−0.291831	−0.26463
H15	0.163897	0.21352
H16	0.125631	0.17349
H17	0.064210	0.13383
H18	0.009451	0.03430
H19	0.077755	0.15795
H20	0.227891	0.34381
H21	0.235197	0.33205

TABLE 8

Vibrational assignments, infrared intensities, Raman activities and Raman intensity of 1A4MPbased on HF and B3LYP/6–311+G(d,p).

Observed frequencies cm^{-1}		Calculated frequencies cm^{-1}				Reduced mass (amu)		Force constant (mdyne A^{-1})		IR intensity (km) mol^{-1}		Raman activity A^0 (amu)		Raman intensity (km) mol^{-1}		Assignments/(%PED)
FTIR	FT-Raman	Unscaled		Scaled												
		a	b	a	b	a	b	a	b	a	b	a	b	a	b	
3390		3803	3549	3416	3389	1.09	1.09	9.31	8.07	3.54	2.22	67.58	93.09	12.82	14.91	$\nu\ NH_{2\ ass}$(100)
	3270	3700	3422	3324	3268	1.05	1.05	8.48	7.27	3.60	11.72	77.88	91.71	16.34	16.24	$\nu\ NH_{2ss}$(100)
	3015	3259	3108	2928	2997	1.10	1.10	6.88	6.26	33.23	20.57	89.15	93.17	28.61	25.24	CH_{2ss}(97)
3007		3236	3093	2907	2988	1.10	1.10	6.81	6.22	51.38	28.95	83.11	78.42	27.43	21.85	CH_{2ass}(98)
2978		3227	3078	2899	2958	1.11	1.11	6.79	6.17	51.86	32.93	69.53	82.54	23.31	23.36	$CH_{3\ ass}$(95)
2954	2952	3207	3054	2881	2935	1.08	1.08	6.56	5.93	65.76	63.18	299.64	315.41	97.53	90.23	$CH_{3\ ass}$(90)
		3200	3050	2875	2931	1.08	1.08	6.54	5.91	92.71	44.77	50.37	56.47	17.16	16.24	CH_{2ss}(97)
		3195	3049	2870	2930	1.07	1.08	6.45	5.91	34.30	32.24	30.00	37.77	10.30	10.94	CH_{2ass}(96)
		3186	3034	2862	2916	1.07	1.07	6.41	5.79	36.21	38.30	76.69	115.61	26.51	33.75	CH_{2ss}(97)
2920	2901	3179	3028	2856	2910	1.06	1.06	6.34	5.74	13.13	15.54	43.66	44.90	16.12	14.00	$CH_{3\ ss}$(85)
	2818	3079	2908	2766	2806	1.06	1.06	5.94	5.30	168.64	156.07	198.98	209.26	76.60	68.01	$CH_{2\ ass}$(97)
	2783	3064	2891	2753	2776	1.07	1.07	5.92	5.28	33.95	49.90	27.34	55.52	10.73	18.40	CH_{2ass}(98)
	2775	3041	2860	2732	2748	1.07	1.07	5.85	5.17	53.79	70.06	40.64	65.22	32.42	43.92	CH_{2ss}(97)
1586	1583	1822	1675	1637	1575	1.09	1.08	2.12	1.78	25.37	20.48	2.87	5.17	4.21	6.40	NH_{2sciss}(91)+ $\nu\ R_{ring}$(39)
1459	1438	1638	1507	1472	1417	1.11	1.06	1.76	1.42	8.38	7.44	4.52	13.99	7.41	19.36	$\delta\ CH_{3\ sb}$ (86)
1411	1415	1628	1506	1463	1416	1.06	1.09	1.66	1.46	4.23	8.90	14.17	8.86	23.47	12.39	CH_{2sciss}(85)
		1620	1490	1455	1432	1.09	1.08	1.68	1.41	2.22	0.36	0.20	3.16	0.33	4.46	CH_{2sciss}(82)
		1611	1486	1447	1428	1.11	1.05	1.69	1.36	5.56	18.41	2.53	5.40	4.26	7.67	$\delta\ CH_{3ipb}$(72)
		1610	1478	1446	1420	1.05	1.10	1.60	1.41	14.83	7.64	5.47	2.24	9.27	3.21	CH_{2sciss}(79)
		1596	1464	1434	1407	1.09	1.09	1.64	1.37	2.79	5.78	9.61	9.26	16.53	13.45	CH_{2sciss}(82)
	1383	1585	1456	1424	1399	1.23	1.20	1.83	1.50	0.77	0.13	2.43	4.29	4.28	6.38	ν N-NH_2(75)
1320	1321	1551	1402	1393	1318	1.65	1.45	2.34	1.68	5.36	7.24	1.50	2.47	2.73	3.80	$\delta CH_{3\ opb}$ (85)
		1530	1389	1374	1306	1.52	1.35	2.10	1.54	24.93	12.15	0.36	1.95	0.67	3.06	ν CN(45)
		1517	1378	1363	1295	1.45	1.35	1.96	1.51	10.38	5.03	0.45	0.87	0.86	1.40	$CH_{2\ rock}$(76)
		1487	1359	1336	1278	1.41	1.33	1.84	1.45	0.75	0.49	2.23	1.59	4.34	2.61	$CH_{2\ rock}$(73)
1275	1271	1483	1357	1332	1276	1.36	1.41	1.76	1.53	0.28	0.23	2.15	3.70	4.28	6.22	ν CN (48) + ν NN(27)
1243	1241	1442	1320	1295	1241	1.86	1.49	2.27	1.53	30.88	20.71	0.74	2.20	1.53	3.84	ν CN (46) + ν NN(40)
		1425	1308	1280	1230	1.34	1.40	1.60	1.41	10.63	11.56	9.72	10.69	20.34	18.88	$CH_{2\ twist}$(68)
		1423	1304	1278	1226	1.27	1.27	1.52	1.27	7.47	5.36	0.38	1.78	0.81	3.22	$CH_{2\ rock}$(65)
1179	1188	1379	1257	1239	1182	1.74	1.84	1.95	1.71	3.27	6.43	2.95	2.25	6.73	4.33	$CH_{2\ rock}$(72)
1138	1146	1316	1211	1182	1138	1.18	1.18	1.20	1.02	0.40	0.94	3.20	3.46	7.71	7.04	$CH_{2\ twist}$(75)

1091		1301	1182	1169	1111	1.96	1.99	1.96	1.63	5.12	4.51	5.43	4.07	13.38	8.47	$CH_{2\ twist}$(68)
1090		1279	1166	1149	1096	2.21	2.64	2.13	2.12	14.26	40.28	2.84	7.09	7.14	15.06	$CH_{2\ twist}$(63)
1074	1076	1272	1153	1143	1084	2.51	2.47	2.39	1.94	50.54	13.34	9.47	2.85	24.50	6.23	$NH_{2\ rock}$(69)
1046	1042	1226	1122	1101	1055	1.44	1.58	1.27	1.17	16.98	12.98	1.24	1.42	3.42	3.31	δ $CH_{3\ ipr}$ (85)
1022	1038	1170	1074	1051	1010	1.85	1.78	1.49	1.21	13.22	15.03	4.75	2.51	13.79	6.15	δ $CH_{3\ opr}$ (84)
	990	1164	1062	1046	998	1.75	2.05	1.39	1.36	1.28	4.84	4.26	4.68	12.49	11.59	$CH_{2\ wagg}$(75)+ ν NN(30)
		1154	1054	1037	991	1.73	1.83	1.36	1.20	16.08	13.04	0.66	0.42	1.99	1.07	$CH_{2\ wagg}$(71)
949	958	1118	1031	1004	969	2.25	2.31	1.66	1.45	20.03	26.74	1.25	0.98	3.98	2.63	δ_{ring}(21)+ δ N-CH_3(18)
	896	1071	986	962	919	2.14	2.30	1.45	1.32	28.87	27.76	5.97	6.51	20.40	18.78	ν CC (51)
848		1014	914	911	852	1.73	2.27	1.05	1.12	56.69	4.52	0.75	0.48	2.77	1.50	ν CC (53)
	833	970	879	871	819	1.96	1.77	1.09	0.80	47.64	66.45	0.15	1.42	0.60	4.78	$CH_{2\ wagg}$(74)
788	792	906	831	814	775	1.60	1.63	0.77	0.66	0.13	0.25	2.09	1.22	9.13	4.50	$NH_{2\ wagg}$(69)
		863	781	775	761	3.10	2.90	1.36	1.04	28.46	15.67	3.40	7.64	15.78	29.93	ν CN(45)+ ν NN(37)
730	714	844	772	758	720	3.47	4.18	1.46	1.47	5.96	24.76	19.64	8.25	98.00	35.46	ν N-CH3 (65)
566	563	695	642	624	598	2.08	2.09	0.59	0.51	9.54	11.78	1.41	3.06	9.45	17.32	$CH_{2\ wagg}$(58)
474	474	558	517	501	482	2.82	2.83	0.52	0.45	4.54	3.99	1.33	1.73	11.70	12.85	$\gamma_{\ ring}$(24)
460		519	482	466	449	2.40	2.39	0.38	0.33	1.05	1.60	1.52	1.08	14.79	8.87	γ NH_2(58)+ $\gamma_{\ ring}$(26)
		489	454	439	443	2.22	2.15	0.31	0.26	8.17	9.35	0.90	0.78	9.63	7.04	γ CN(19)
	368	442	413	397	403	2.84	2.82	0.33	0.28	1.50	1.67	1.49	1.92	18.47	20.09	δ CNC(21)+ δ NH_2(20)
		399	368	358	359	2.09	2.05	0.20	0.16	7.95	6.74	1.39	2.81	19.82	33.82	γ_{ring}(28)
		385	357	346	348	2.21	2.17	0.19	0.16	0.28	0.32	0.01	0.05	0.15	0.65	δ CNN(39)
	298	335	325	301	317	1.06	1.07	0.07	0.07	44.90	40.02	0.24	0.49	4.57	7.88	τ NH_2 (81)
		268	257	241	250	1.43	1.33	0.06	0.05	1.37	1.01	0.30	0.52	7.95	11.64	δ_{ring}(19)
	223	251	233	225	227	2.35	2.57	0.09	0.08	4.02	4.52	0.18	0.18	5.31	4.48	γ CN (28)
	172	231	216	208	211	1.63	1.69	0.05	0.05	0.34	0.21	0.28	0.36	9.81	10.65	$\gamma_{\ ring}$(25)
		127	116	114	113	3.08	3.11	0.03	0.02	0.22	0.21	0.69	1.20	68.11	98.00	τ CH_3(35)

ν, stretching; ss, symmetric stretching; ass, asymmetric stretching; δ, in-plane bending; γ, out-of-plane bending; sciss, scissoring; wag., wagging; rock, rocking; ipb, inplanebending; opb, out-of-plane bending, ipr, in-plane rocking; opr, out-of-plane rocking; twist, twisting; δring, ring in-plane-bending; γring, ring out-of-plane-bending.

[a] Calculated by HF/6-311+G(d,p).

[b] Calculated by B3LYP/6-311+G(d,p).

TABLE 9

Theoretical electronic absorption spectra of 1A4MP (absorption wavelength λ (nm), excitation energies E(eV) and oscillator strengths (*f*)) using TD-DFT/B3LYP/6-31+G(d,p) method in gas and solvent(DMSO and acetone) phase.

Excitation level	Gas			DMSO			Acetone		
	max(nm)	ΔE(eV)	*f*	max(nm)	ΔE(eV)	*f*	max(nm)	ΔE(eV)	*f*
H– L	365.58	3.3915	0.0351	348.31	3.5596	0.0385	348.58	3.5568	0.0367
H1– L1	327.27	3.7884	0.1021	322.65	3.8427	0.1517	322.43	3.8453	0.1489
H2–L1	319.43	3.8814	0.0153	303.82	4.0808	0.0291	304.47	4.0722	0.0276

HIGHLIGHTS

- FT-IR and Raman spectra of 1-Amino-4-methylpiperazine were recorded and analyzed.
- The complete vibrational assignments and spectroscopic analysis were made.
- The HOMO, LUMO energy gap were theoretically predicted.
- Stability, charge delocalization analyzed by using NBO theory.
- Electrostatic potential of 1-Amino4-methylpiperazine was calculated.

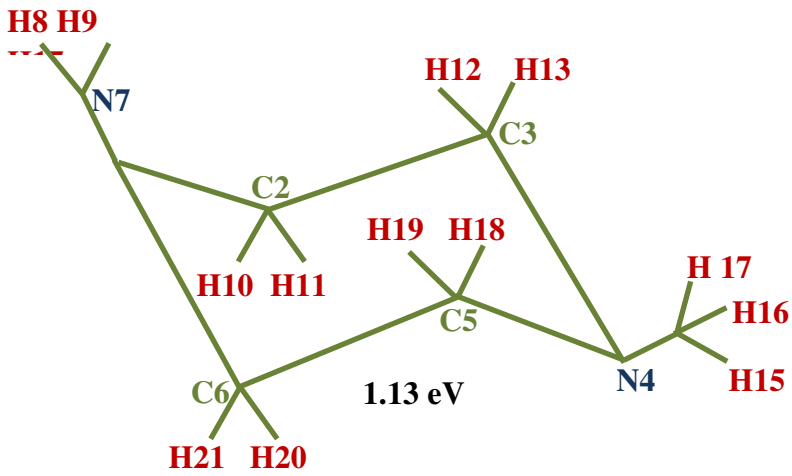

cis - cis(I)

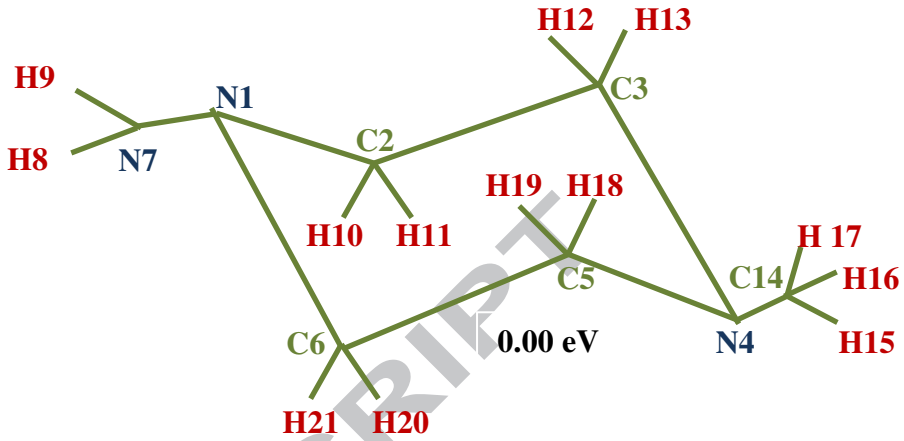

trans - cis(III)

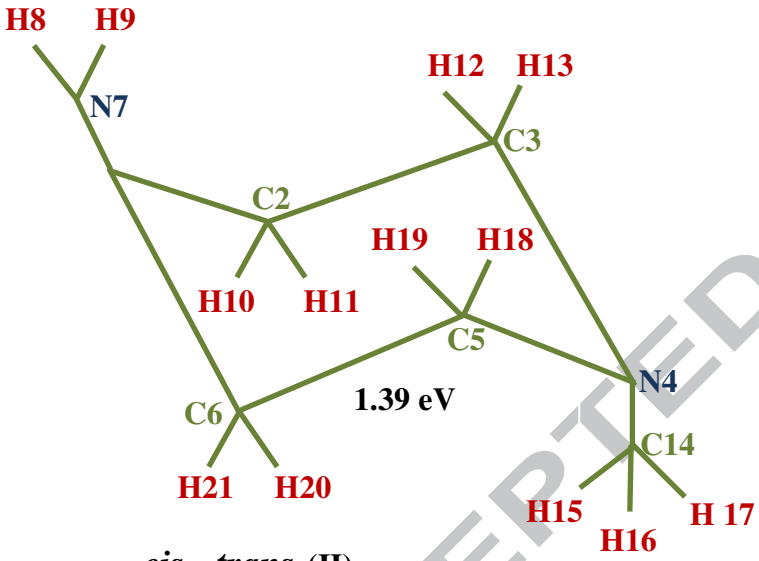

cis - trans (II)

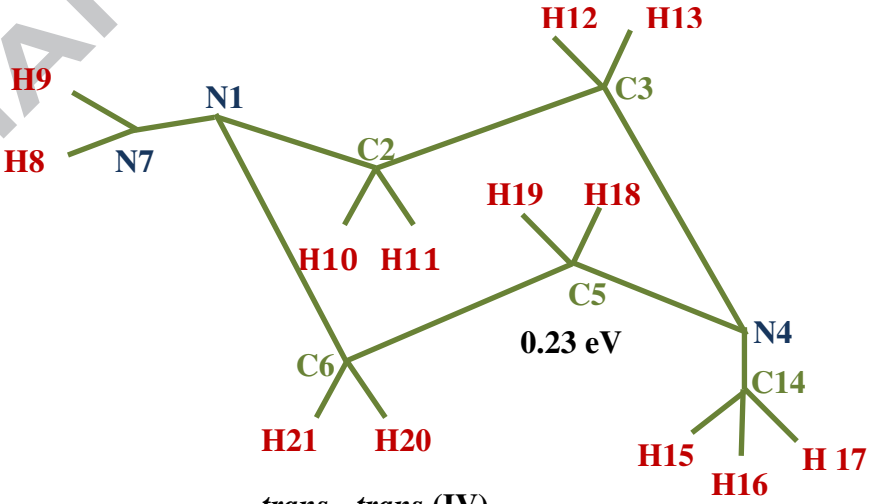

trans - trans (IV)